

Fault-Tolerant Multi-Modal Localization of Multi-Robots on Matrix Lie Groups

Mahboubeh Zarei and Robin Chhabra, *Senior Member, IEEE*,

Abstract—Consistent localization of cooperative multi-robot systems during navigation presents substantial challenges. This paper proposes a fault-tolerant, multi-modal localization framework for multi-robot systems on matrix Lie groups. We introduce novel stochastic operations to perform composition, differencing, inversion, averaging, and fusion of correlated and non-correlated estimates on Lie groups, enabling pseudo-pose construction for filter updates. The method integrates a combination of proprioceptive and exteroceptive measurements from inertial, velocity, and pose (pseudo-pose) sensors on each robot in an Extended Kalman Filter (EKF) framework. The prediction step is conducted on the Lie group $\mathbb{SE}_2(3) \times \mathbb{R}^3 \times \mathbb{R}^3$, where each robot's pose, velocity, and inertial measurement biases are propagated. The proposed framework uses body velocity, relative pose measurements from fiducial markers, and inter-robot communication to provide scalable EKF update across the network on the Lie group $\mathbb{SE}(3) \times \mathbb{R}^3$. A fault detection module is implemented, allowing the integration of only reliable pseudo-pose measurements from fiducial markers. We demonstrate the effectiveness of the method through experiments with a network of wheeled mobile robots equipped with inertial measurement units, wheel odometry, and ArUco markers. The comparison results highlight the proposed method's real-time performance, superior efficiency, reliability, and scalability in multi-robot localization, making it well-suited for large-scale robotic systems.

I. INTRODUCTION

MOBILE robots, whether operating individually or as part of a team, are widely deployed in indoor environments to perform a variety of tasks, such as inspection, source searching, delivery, and quality control [1], [2]. Fully autonomous navigation of mobile robots requires accurate, fast, and cost-effective localization systems, optimized by careful selection of motion sensors, information exchange strategies, and computing algorithms. Over the past few decades, numerous localization methods have emerged, integrating proprioceptive and exteroceptive sensors. Inertial odometry, relying on proprioceptive inertial sensors such as accelerometers, gyroscopes, magnetometers, and Inertial Measurement Units (IMUs), provides a simple and self-contained solution [3]. However, it faces challenges especially in translational directions of motion due to the well-known noise propagation problem in accelerometers [3], [4]. To mitigate these errors, velocity measurements—such as those from encoders or optical flow sensors—can be fused with inertial data within a sensor fusion framework [5]–[8]. However, these methods

still struggle to provide precise estimates due to environmental factors and inherent systematic errors. As a result, periodic exteroceptive position updates using sensors such as camera, Ultra-WideBand (UWB), and LiDAR are essential to maintaining accuracy in a multi-sensor fusion framework [9]–[11]. In a multi-robot localization problem, providing pose updates to all agents is often impractical or costly. Alternatively, we can leverage pose updates of neighboring agents to significantly enhance robots' localization via enabling inter-robot communication. Accordingly, leader-follower (collaborative) localization has emerged as a robust and scalable solution [12]–[15]. In this approach, a subset of robots, known as leaders, access accurate global localization information, which is shared with the rest of the robots (followers), improving their pose estimates. Computational algorithms are the last key aspect of the localization system design that are categorized into estimation-based and optimization-based approaches. The estimation-based approaches such as Extended Kalman Filter (EKF) offer significant advantages in handling uncertainty, fusing data from multiple sensors, providing real-time updates, and enabling cost-effective computations [16]. Moreover, they are highly scalable, making them well-suited for multi-robot systems [17]. Robots' motion is rigorously captured on the Special Euclidean Lie Group $\mathbb{SE}(3)$, whose elements provide an unambiguous pose representation unlike Euler angles and quaternions [18], removing the need for calculating intricate Jacobians of representation maps. Implementing Lie groups in the estimation process, however, necessitates systematic representation of uncertainty on these nonlinear spaces.

Building upon foundational concepts of pose representation and sensor fusion for localization within the framework of matrix Lie groups, this paper first develops stochastic operations on matrix Lie groups, followed by the presentation of a multi-robot multi-sensor localization system that fuses inertial, velocity, and pose data. To scale the method to include multiple robots, we assume access to global and relative pose information using an exteroceptive sensor such as fiducial markers. In the following section, we explore techniques for estimation and fusion on matrix Lie groups and review relevant works on multi-sensor and multi-robot localization.

A. Related works

1) *Estimation on Matrix Lie Groups*: Localization of systems evolving on matrix Lie groups centers around characterizing random pose variables on matrix Lie groups and their associated Lie algebras. The use of differential homogeneous transformations to represent uncertainty on Special Euclidean

M. Zarei is with the Autonomous Space Robotics and Mechatronics Laboratory, Carleton University, Ottawa, ON, Canada.

R. Chhabra is with the Mechanical, Industrial, and Mechatronics Engineering Department, Toronto Metropolitan University, Toronto, ON, Canada.

These studies laid the groundwork for handling uncertainty propagation in the context of rigid body motion, with an emphasis on matrix representations of spatial transformations. A more comprehensive framework for expressing and advancing uncertainty on matrix Lie groups is presented in [22]–[24].

Recent work by Long *et al.* demonstrated that the observed probability distributions on $\mathbb{SE}(n)$ are normal in the exponential coordinates [25]. This result offers valuable insights into using exponential maps for uncertainty propagation in localization, as the estimation framework can accommodate higher errors without concern for the breakdown of the normality assumption in the presence of high uncertainties. Building on these advancements, Barfoot *et al.* [26] proposed a framework for capturing pose uncertainties in the Lie algebra and using the exponential map to propagate these uncertainties for discrete-time variables on $\mathbb{SE}(n)$. This method was then extended to capture continuous-time random variables on $\mathbb{SE}(3)$ [27], [28]. To complete the requirements of pose estimation, Mangelson *et al.* enabled operations on two correlated pose estimates, such as composition, inversion, and relative pose, while accounting for uncertainties in the Lie algebra [29]. These advancements have facilitated the development of consistent and efficient estimation solutions, such as the Extended Kalman Filter (EKF) on Lie groups [30], [31], the Invariant EKF (IEKF) [32], [33], the Unscented Kalman Filter (UKF) on Lie groups [34], [35], particle filters on Lie groups [36], and preintegration methods [37].

Fusion of stochastic poses is a critical operation in the localization of robots, especially in scenarios where estimates from different robots are available. Excluding cross-correlations, Drummond *et al.* [38] and Barfoot *et al.* [26] explored iterative naive methods to combine two and multiple pose estimates, respectively. Non-iterative naive solutions for combining multiple poses on $\mathbb{SE}(3)$ have been introduced in [25], [39]–[41]. To address cross-correlations, Li *et al.* [42] presented a conservative iterative method that extends the split Covariance Intersection (CI) approach to matrix Lie groups. Accordingly, conservative distributed IEKF solutions based on CI were developed in [43] and [33]. Recently, [44] proposed a non-iterative fusion method for multiple pose estimates that ensures consistency by propagating and incorporating cross-correlations.

2) *Multi-robot Localization on Lie Groups*: Many localization methods for robots have been developed that rely on sensor fusion techniques such as EKF or UKF, using inertial and visual sensors [31], [45], [46], inertial sensor and Global Navigation Satellite System (GNSS) [47], or inertial and velocity measurements [48]. However, their extension to multi-robot systems is not straightforward and requires consideration of communication constraints in the network of robots, combining information from sensors with different modalities, and computational efficiency. Recent studies have explored various approaches to address these challenges. For instance, Li and Chirikjian [49] proposed decentralized localization frameworks for multiple robots based on a second-order sensor fusion technique, focusing on how the geometry of $\mathbb{SE}(3)$ can improve the localization performance. The method can be computationally expensive as the computation increases

with the number of measurements taken and the technique is susceptible to error accumulation when no neighboring robot has an accurate pose estimate. Dubois *et al.* [50], [51] used visual and inertial sensors to enable decentralized collaborative Simultaneous Localization and Mapping (SLAM) that improves pose estimation by designing of efficient data sharing methods. However, this method has the potential to drift especially when dealing with featureless areas, low lighting conditions, or rapid motion, which can lead to inaccurate map building and localization. Moreover, it is computationally expensive, requiring significant processing power and resources to operate in real-time. Knuth and Barooah [52] proposed a model-free distributed framework on $\mathbb{SE}(3)$ for localization of a multi-robot system based on relative poses from the neighboring robots in a GPS-denied environment. The method was evaluated by numerical simulations and there is no analytical guarantee on the performance. Shin *et al.* [53] proposed a multi-robot pose estimation framework on $\mathbb{SE}(2)$, with a particular focus on the observability analysis of relative pose estimation. They compared the performance of method utilizing EKF and pose graph optimization, both relying on relative pose data obtained from UWB sensors. To address the inconsistencies of classical distributed EKF on Euclidean spaces, Xu *et al.* [43] proposed a CI-based distributed IEKF for cooperative target tracking on $\mathbb{SE}_2(3)$, although they overlooked relative noise and IMU biases. Moreover, the IEKF has been applied to distributed cooperative localization [54] and multi-robot object-level pose SLAM [55].

3) *Fiducial Marker-based Pose Estimate* : Fiducial markers such as ArUco and AprilTag offer a simple, reliable and cost-effective means to update pose in structured settings [56]. Marker poses can be used directly or fused with other sensor data in the filter update step [57]–[59]. The benefit of fiducial markers is their ability to easily obtain relative pose measurements between robots without relying on external sources. Accordingly, several multi-robot navigation frameworks have been proposed. For example, Joon *et al.* proposed a leader-follower control system with estimation-based localization [60] in which multiple ArUco markers are installed on the leader and the follower robot employs a rotating camera to detect them. Localization is achieved by fusing IMU, encoder, and ArUco pose data through two EKFs for the follower and one for the leader. Zhou *et al.* in [61] presented a cooperative multi-robot localization, utilizing real-time communication and a two-stage EKF that fuses IMU and encoder data with relative pose measurements obtained from the ArUco marker on the follower robot. In [62], a marker-based cooperative localization method is introduced that mimics caterpillar-like motion. It combines absolute pose estimates from static features with relative pose estimates from mobile fiducial markers, framed as an online optimization problem integrating two objectives from different feature sources. Shan *et al.* [63] proposed a Bayesian leader-follower trajectory estimation, where the follower estimates the leader's trajectory using noisy odometry data and relative fiducial marker observations. The leader-follower formation problem based on the relative pose measurements of the leader was introduced in [64], while [65] proposed a control law for

cooperative object handling in a leader-follower system. All of the aforementioned works were developed within Euclidean spaces and are limited to networks of size two, or leader-follower frameworks.

B. Contributions

This paper proposes stochastic operations for multiple correlated and uncorrelated estimates on Lie groups and uses them to advance a fault-tolerant, multi-modal localization method for multi-robot systems evolving on matrix Lie groups. Each robot in the network runs an EKF to fuse inertial measurements on the proposed manifold $\mathbb{SE}_2(3) \times \mathbb{R}^3 \times \mathbb{R}^3$ with high-frequency velocity measurements on \mathbb{R}^3 or velocity and pseudo-pose data on a measurement manifold of $\mathbb{SE}(3) \times \mathbb{R}^3$. Using relative pose information, inter-robot communications, and developed stochastic operations, the proposed estimation framework enables scalable collaborative localization across all robots in the network. Thus, the key contributions of this work are as follows:

- (i) This paper proposes stochastic operations on an arbitrary matrix Lie group. In contrast to previous approaches [26], [29], the operations are not limited to poses, batch formulas are developed for multiple correlated estimates, and new operations such as constrained fusion and averaging are considered.
- (ii) We present a new practical multi-robot multi-modal localization method on Lie groups, which, unlike [49], [50], [53], fuses inertial measurements on $\mathbb{SE}_2(3) \times \mathbb{R}^3 \times \mathbb{R}^3$ with velocity and pose data on $\mathbb{SE}(3) \times \mathbb{R}^3$. In contrast to previous approaches limited to two robots [60]–[63], our method scales cooperative localization across the entire robotic network considering three types of robots: leader, follower type 1 and follower type 2. It also integrates a fault detection module on each robot's local filter to identify the reliable pose measurements.
- (iv) We conducted experiments on a network of wheeled mobile robots to evaluate the localization system, combining IMU data with velocity measurements from wheel encoders and pseudo-pose measurements obtained from ArUco markers.

II. PRELIMINARIES

A. Matrix Lie groups in Robotics

Here, the extended pose that encompasses vectors such as velocity and landmark positions, is described by a matrix $\mathcal{X} \in \mathbb{R}^{\kappa+3 \times \kappa+3}$ that belongs to the κ -Direct Isometries group [66]:

$$\mathbb{SE}_\kappa(3) := \left\{ \mathcal{X} = \begin{bmatrix} \mathcal{R} & \mathbf{p}_1 & \mathbf{p}_2 & \cdots & \mathbf{p}_\kappa \\ \mathbf{0}_{3 \times 1}^\top & 1 & 0 & \cdots & 0 \\ \mathbf{0}_{3 \times 1}^\top & 0 & 1 & \cdots & 0 \\ \vdots & \vdots & \vdots & \ddots & \vdots \\ \mathbf{0}_{3 \times 1}^\top & 0 & 0 & \cdots & 1 \end{bmatrix} \middle| \mathcal{R} \in \mathbb{SO}(3), \mathbf{p}_i \in \mathbb{R}^3 \right\}, \quad (1)$$

where \mathbf{p}_i , $i \in \{1, \dots, \kappa\}$, is a translation vector with respect to some reference frame, and \mathcal{R} is a rotation matrix that belongs to the Special Orthogonal group $\mathbb{SO}(3) := \{\mathcal{R} \in \mathbb{R}^{3 \times 3} | \mathcal{R}\mathcal{R}^\top = \mathbf{I}_3, \det(\mathcal{R}) = 1\}$. Here, \mathbf{I}_n and $\mathbf{0}_n$

denote an n -dimensional identity matrix and zero matrix, respectively. Note that for $\kappa = 0$ and $\kappa = 1$ the group $\mathbb{SE}_\kappa(3)$ reduces to $\mathbb{SO}(3)$ and $\mathbb{SE}(3)$, respectively. The tangent space at the identity element $\mathbf{I}_{\kappa+3}$ along with a bracket operator (commutator) forms the Lie algebra $\mathfrak{se}_\kappa(3)$:

$$\mathfrak{se}_\kappa(3) := \left\{ [\zeta]_\wedge = \begin{bmatrix} [\varphi]_\times & \rho_1 & \rho_2 & \cdots & \rho_\kappa \\ \mathbf{0}_{3 \times 1}^\top & 0 & 0 & \cdots & 0 \\ \mathbf{0}_{3 \times 1}^\top & 0 & 0 & \cdots & 0 \\ \vdots & \vdots & \vdots & \ddots & \vdots \\ \mathbf{0}_{3 \times 1}^\top & 0 & 0 & \cdots & 0 \end{bmatrix} \in \mathbb{R}^{\kappa+3 \times \kappa+3} \middle| \varphi, \rho_i \in \mathbb{R}^3 \right\},$$

where the operator $[\cdot]_\wedge$ indicates the isomorphism between $\mathbb{R}^{3+3\kappa}$ and $\mathfrak{se}_\kappa(3)$, with the inverse operator being denoted by $[\cdot]_\vee$. That is, $\zeta = [\varphi \ \rho_1 \ \rho_2 \ \cdots \ \rho_\kappa]^\top \in \mathbb{R}^{3+3\kappa}$. Moreover, the operator $[\cdot]_\times$ generates the skew-symmetric matrix of the vector φ and $[\cdot]_\otimes$ does the inverse.

The exponential map $\exp : \mathfrak{se}_\kappa(3) \rightarrow \mathbb{SE}_\kappa(3)$ maps a Lie algebra element $[\zeta]_\wedge \in \mathfrak{se}_\kappa(3)$ to an element $\mathcal{X} \in \mathbb{SE}_\kappa(3)$ whose inverse is called the logarithm mapping $\log : \mathbb{SE}_\kappa(3) \rightarrow \mathfrak{se}_\kappa(3)$, with explicit forms:

$$\mathcal{X} = \exp([\zeta]_\wedge) = \begin{bmatrix} \exp([\varphi]_\times) & \mathbf{V}(\varphi)\rho_1 & \mathbf{V}(\varphi)\rho_2 & \cdots & \mathbf{V}(\varphi)\rho_\kappa \\ \mathbf{0}_{3 \times 1}^\top & 1 & 0 & \cdots & 0 \\ \mathbf{0}_{3 \times 1}^\top & 0 & 1 & \cdots & 0 \\ \vdots & \vdots & \vdots & \ddots & \vdots \\ \mathbf{0}_{3 \times 1}^\top & 0 & 0 & \cdots & 1 \end{bmatrix},$$

$$\zeta = [\log(\mathcal{X})]_\vee = \begin{bmatrix} [\log(\mathcal{R})]_\otimes \\ \mathbf{V}^{-1}([\log(\mathcal{R})]_\otimes)\mathbf{p}_1 \\ \mathbf{V}^{-1}([\log(\mathcal{R})]_\otimes)\mathbf{p}_2 \\ \vdots \\ \mathbf{V}^{-1}([\log(\mathcal{R})]_\otimes)\mathbf{p}_\kappa \end{bmatrix}.$$

Here, for non-zero $\phi := \|\varphi\| \neq 0$, it is derived [23]:

$$\mathbf{V}(\varphi) = \mathbf{I}_3 + \frac{1 - \cos \phi}{\phi^2} [\varphi]_\times + \frac{\phi - \sin \phi}{\phi^3} [\varphi]_\times^2, \quad (2)$$

$$\mathbf{V}^{-1}(\varphi) = \mathbf{I}_3 - \frac{1}{2} [\varphi]_\times + \left(\frac{1}{\phi^2} - \frac{1 + \cos \phi}{2\phi \sin \phi} \right) [\varphi]_\times^2, \quad (3)$$

$$\mathcal{R} = \exp([\varphi]_\times) = \mathbf{I}_3 + \frac{\sin \phi}{\phi} [\varphi]_\times + \frac{1 - \cos \phi}{\phi^2} [\varphi]_\times^2, \quad (4)$$

and when $\phi = 0$, we have $\mathcal{R} = \mathbf{V}(\varphi) = \mathbf{I}_3$. Moreover, for $\psi = \cos^{-1}(\frac{\text{tr}(\mathcal{R})-1}{2})$, we have $\varphi = [\log(\mathcal{R})]_\otimes = \left[\frac{\psi}{2 \sin \psi} (\mathcal{R} - \mathcal{R}^\top) \right]_\otimes$.

For an element $\mathcal{X} \in \mathbb{SE}_\kappa(3)$, the Adjoint $\text{Ad}_\mathcal{X} : \mathfrak{se}_\kappa(3) \rightarrow \mathfrak{se}_\kappa(3)$ is defined as a mapping that represents the conjugate action of $\mathbb{SE}_\kappa(3)$ on its Lie algebra, i.e., $\text{Ad}_\mathcal{X}(\zeta) := [\mathcal{X} [\zeta]_\wedge \mathcal{X}^{-1}]_\vee$. Thus, the Adjoint representation of $\mathbb{SE}_\kappa(3)$ takes the matrix form [23], [67]:

$$\text{Ad}_\mathcal{X} = \begin{bmatrix} \mathcal{R} & \mathbf{0}_3 & \mathbf{0}_3 & \cdots & \mathbf{0}_3 \\ [\mathbf{p}_1]_\times & \mathcal{R} & \mathcal{R} & \mathbf{0}_3 & \cdots & \mathbf{0}_3 \\ [\mathbf{p}_2]_\times & \mathcal{R} & \mathbf{0}_3 & \mathcal{R} & \cdots & \mathbf{0}_3 \\ \vdots & \vdots & \vdots & \ddots & \vdots & \vdots \\ [\mathbf{p}_\kappa]_\times & \mathcal{R} & \mathbf{0}_3 & \mathbf{0}_3 & \cdots & \mathcal{R} \end{bmatrix} \in \mathbb{R}^{3\kappa+3 \times 3\kappa+3}. \quad (5)$$

For the vector ζ , we can also define the adjoint representation of the Lie algebra $\mathfrak{se}_\kappa(3)$ with the mapping $\text{ad}_\zeta : \mathfrak{se}_\kappa(3) \rightarrow \mathfrak{se}_\kappa(3)$ defined by

$$\text{ad}_\zeta(\eta) := [[\zeta]_\wedge, [\eta]_\wedge]_\vee = [[\zeta]_\wedge [\eta]_\wedge - [\eta]_\wedge [\zeta]_\wedge]_\vee, \quad (6)$$

where $[\zeta]_{\wedge}, [\eta]_{\wedge} \in \mathfrak{se}_{\kappa}(3)$ and $[\cdot, \cdot]$ is the commutator operator. This map in its matrix form is as follows:

$$\mathbf{ad}_{\zeta} = \begin{bmatrix} [\varphi]_{\times} & \mathbf{0}_3 & \mathbf{0}_3 & \cdots & \mathbf{0}_3 \\ [\rho_1]_{\times} & [\varphi]_{\times} & \mathbf{0}_3 & \cdots & \mathbf{0}_3 \\ [\rho_2]_{\times} & \mathbf{0}_3 & [\varphi]_{\times} & \cdots & \mathbf{0}_3 \\ \vdots & \vdots & \vdots & \ddots & \vdots \\ [\rho_{\kappa}]_{\times} & \mathbf{0}_3 & \mathbf{0}_3 & \cdots & [\varphi]_{\times} \end{bmatrix} \in \mathbb{R}^{3\kappa+3 \times 3\kappa+3}. \quad (7)$$

B. The Baker–Campbell–Hausdorff (BCH) Formula

Let $\mathcal{X} = \exp([\zeta]_{\wedge}) \in \mathbb{SE}_{\kappa}(3)$ and $\mathcal{Y} = \exp([\eta]_{\wedge}) \in \mathbb{SE}_{\kappa}(3)$, where $[\zeta]_{\wedge}, [\eta]_{\wedge} \in \mathfrak{se}_{\kappa}(3)$. If

$$\exp([\lambda]_{\wedge}) := \mathcal{X}\mathcal{Y} = \exp([\zeta]_{\wedge}) \exp([\eta]_{\wedge}), \quad (8)$$

then based on the BCH formula [67],

$$\lambda = \zeta + \eta + \frac{1}{2} \mathbf{ad}_{\zeta} \eta + \frac{1}{12} \mathbf{ad}_{\zeta} \mathbf{ad}_{\zeta} \eta + \frac{1}{12} \mathbf{ad}_{\eta} \mathbf{ad}_{\eta} \zeta + \cdots \quad (9)$$

For small values of η , it is shown in [68] that

$$\lambda \approx \zeta + \mathcal{J}_r^{-1}(\zeta) \eta, \quad (10)$$

where the right Jacobian of $\mathbb{SE}_{\kappa}(3)$ for non-zero rotation angles is [23], [68]:

$$\begin{aligned} \mathcal{J}_r(\zeta) &= \mathbf{I}_{3\kappa+3} - \frac{4 - \phi \sin(\phi) - 4 \cos(\phi)}{2\phi^2} \mathbf{ad}_{\zeta} \\ &+ \frac{4\phi - 5 \sin(\phi) + \phi \cos(\phi)}{2\phi^3} \mathbf{ad}_{\zeta}^2 \\ &- \frac{2 - \phi \sin(\phi) - 2 \cos(\phi)}{2\phi^4} \mathbf{ad}_{\zeta}^3 \\ &+ \frac{2\phi - 3 \sin(\phi) + \phi \cos(\phi)}{2\phi^5} \mathbf{ad}_{\zeta}^4. \end{aligned}$$

When the rotation angle is zero, $\mathcal{J}_r(\zeta) = \mathbf{I}_{3\kappa+3} + \frac{1}{2} \mathbf{ad}_{\zeta}$.

C. Extended Kalman Filter on Matrix Lie Groups

As illustrated in Fig.1, on an arbitrary Lie group $\mathcal{G}_{\mathcal{X}}$, a stochastic member is defined as $\mathcal{X} = \bar{\mathcal{X}} \exp([\zeta]_{\wedge})$ where $\bar{\mathcal{X}}$ denotes the deterministic part and $\zeta \sim \mathcal{N}(\mathbf{0}_{m \times 1}, \mathbf{P})$ is a zero-mean Gaussian vector with the covariance $\mathbf{P} \in \mathbb{R}^{m \times m}$. Let a discrete-time system on $\mathcal{G}_{\mathcal{X}}$ with noisy measurements from a sensor be [69]:

$$\mathcal{X}^{(k+1)} = \mathcal{X}^{(k)} \exp([\mathbf{f}(\mathcal{X}^{(k)}, \mathbf{u}^{(k)}) + \mathbf{w}^{(k)}]_{\wedge}), \quad (11)$$

$$\mathcal{Z}^{(k)} = \mathbf{h}(\mathcal{X}^{(k)}) \exp([\mathbf{m}^{(k)}]_{\wedge}), \quad (12)$$

where the measurement signal $\mathcal{Z}^{(k)} \in \mathcal{G}_{\mathcal{Z}}$ is on a q -dimensional matrix Lie group according to the model $\mathbf{h} : \mathcal{G}_{\mathcal{X}} \rightarrow \mathcal{G}_{\mathcal{Z}}$ and $\mathbf{u}^{(k)} \in \mathbb{R}^r$ is the control input to the process whose model is described by the function $\mathbf{f} : \mathcal{G}_{\mathcal{X}} \times \mathbb{R}^r \rightarrow \mathbb{R}^m$. The covariance of the normal white noise sequences $\mathbf{w}^{(k)} \sim \mathcal{N}(\mathbf{0}_{m \times 1}, \mathbf{Q}^{(k)})$ and $\mathbf{m}^{(k)} \sim \mathcal{N}(\mathbf{0}_{q \times 1}, \mathbf{R}^{(k)})$ are $\mathbf{Q}^{(k)} \in \mathbb{R}^{m \times m}$ and $\mathbf{R}^{(k)} \in \mathbb{R}^{q \times q}$, respectively. We assume that the measurement and process noise signals are independent, i.e., $\mathbb{E}[\mathbf{m}^{(k)} \mathbf{w}^{\top(l)}] = \mathbf{0}_{q \times m}$.

We revisit the method of discrete-time EKF on Lie groups [70] to set our notation. Given the mean and covariance

at the time $k-1$, represented as $\bar{\mathcal{X}}^{(k-1|k-1)}$ and $\mathbf{P}^{(k-1|k-1)}$, respectively, the prediction step calculates the prior estimates

$$\bar{\mathcal{X}}^{(k|k-1)} = \bar{\mathcal{X}}^{(k-1|k-1)} \exp([\bar{\mathbf{f}}^{(k-1)}]_{\wedge}), \quad (13)$$

$$\begin{aligned} \mathbf{P}^{(k|k-1)} &= \mathcal{F}^{(k-1)} \mathbf{P}^{(k-1|k-1)} \mathcal{F}^{\top(k-1)} \\ &+ \mathcal{J}_r(\bar{\mathbf{f}}^{(k-1)}) \mathbf{Q}^{(k-1)} \mathcal{J}_r^{\top}(\bar{\mathbf{f}}^{(k-1)}), \end{aligned} \quad (14)$$

where $\bar{\mathbf{f}}^{(k-1)} = \mathbf{f}(\bar{\mathcal{X}}^{(k-1|k-1)}, \mathbf{u}^{(k-1)})$ and

$$\mathcal{F}^{(k)} = \mathbf{Ad}_{\exp([\bar{\mathbf{f}}^{(k-1)}]_{\wedge})} + \mathcal{J}_r(\bar{\mathbf{f}}^{(k-1)}) \mathcal{D}^{(k-1)}, \quad (15)$$

$$\mathcal{D}^{(k-1)} = \frac{\partial}{\partial \zeta} \mathbf{f}(\bar{\mathcal{X}}^{(k-1|k-1)} \exp([\zeta]_{\wedge}), \mathbf{u}^{(k-1)}) \Big|_{\zeta=0}. \quad (16)$$

At time step k , the update step is executed based on

$$\bar{\mathcal{X}}^{(k|k)} = \bar{\mathcal{X}}^{(k|k-1)} \exp([\mathbf{K}^{(k)} \nu^{(k)}]_{\wedge}), \quad (17)$$

$$\begin{aligned} \mathbf{P}^{(k|k)} &= \mathcal{J}_r(\mathbf{K}^{(k)} \nu^{(k)}) (\mathbf{I}_m - \mathbf{K}^{(k)} \mathbf{H}^{(k)}) \mathbf{P}^{(k|k-1)} \\ &\mathcal{J}_r^{\top}(\mathbf{K}^{(k)} \nu^{(k)}), \end{aligned} \quad (18)$$

where the innovation $\nu^{(k)}$, the EKF gain, and matrix $\mathcal{H}^{(k)}$ are

$$\nu^{(k)} = [\log(\mathbf{h}^{-1}(\bar{\mathcal{X}}^{(k|k-1)}) \mathcal{Z}^{(k)})]_{\vee}, \quad (19)$$

$$\mathbf{K}^{(k)} = \mathbf{P}^{(k|k-1)} \mathcal{H}^{\top(k)} (\mathcal{H}^{(k)} \mathbf{P}^{(k|k-1)} \mathcal{H}^{\top(k)} + \mathbf{R}^{(k)})^{-1}, \quad (20)$$

$$\mathcal{H}^{(k)} = \frac{\partial}{\partial \zeta} [\log(\mathbf{h}^{-1}(\bar{\mathcal{X}}^{(k|k-1)}) \mathbf{h}(\bar{\mathcal{X}}^{(k|k-1)} \exp([\zeta]_{\wedge})))]_{\vee} \Big|_{\zeta=0}. \quad (21)$$

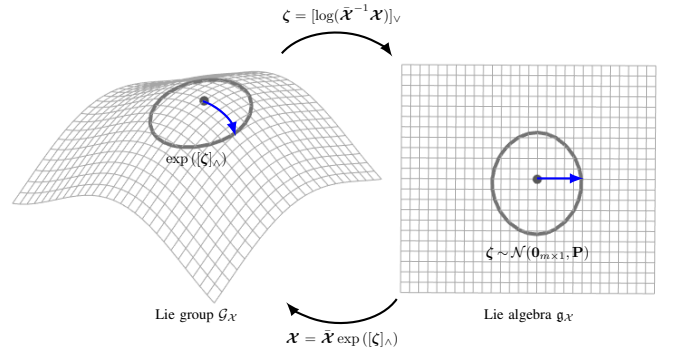


Fig. 1. Uncertainty on Lie group $\mathcal{G}_{\mathcal{X}}$ and its Lie algebra $\mathfrak{g}_{\mathcal{X}}$

III. STOCHASTIC OPERATIONS ON LIE GROUPS

Here, we develop necessary mechanisms to perform fundamental operations on stochastic members of a matrix Lie group. The operations include composition, inverse, difference, averaging, and fusion, which are crucial for the development of our proposed localization algorithm. As shown in Fig. 2, each operation derives an equivalent stochastic member based on the mean and covariance of the input members.

A. Inverse Operation

Let $\mathcal{G}_{\mathcal{X}}$ be an arbitrary Lie group. The inverse operation is illustrated in Fig.2-(a), where for the stochastic member $\mathcal{X} = \bar{\mathcal{X}} \exp([\zeta]_{\wedge}) \in \mathcal{G}_{\mathcal{X}}$ with $\zeta \sim \mathcal{N}(\mathbf{0}_{m \times 1}, \mathbf{P})$, its inverse is defined as $\mathcal{X}_{\text{inv}} = \mathcal{X}^{-1} = \bar{\mathcal{X}}_{\text{inv}} \exp([\zeta]_{\text{inv}}) \in \mathcal{G}_{\mathcal{X}}$ with

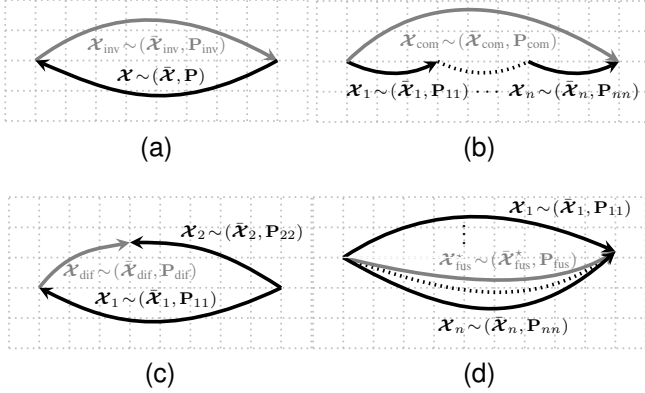


Fig. 2. Illustration of stochastic operations: (a) inverse, (b) composition, (c) difference, and (d) fusion.

$\zeta_{\text{inv}} \sim \mathcal{N}(\mathbf{0}_{m \times 1}, \mathbf{P}_{\text{inv}})$. The mean $\bar{\mathcal{X}}_{\text{inv}} \in \mathcal{G}_{\mathcal{X}}$ and covariance matrix $\mathbf{P}_{\text{inv}} \in \mathbb{R}^{m \times m}$ are calculated as (see Appendix B):

$$\bar{\mathcal{X}}_{\text{inv}} = \bar{\mathcal{X}}^{-1}, \quad (22)$$

$$\mathbf{P}_{\text{inv}} = \text{Ad}_{\bar{\mathcal{X}}} \mathbf{P} \text{Ad}_{\bar{\mathcal{X}}}^{\top}. \quad (23)$$

B. Composition Operation

As shown in Fig.2-(b), let the stochastic member $\mathcal{X}_{\text{com}} \in \mathcal{G}_{\mathcal{X}}$ be composed of

$$\mathcal{X}_{\text{com}} = \mathcal{X}_1 \mathcal{X}_2 \cdots \mathcal{X}_n, \quad (24)$$

where the i^{th} stochastic member is $\mathcal{X}_i = \bar{\mathcal{X}}_i \exp([\zeta_i]_{\wedge}) \in \mathcal{G}_{\mathcal{X}}$ with $\zeta_i \sim \mathcal{N}(\mathbf{0}_{m \times 1}, \mathbf{P}_{ii})$ and non-zero cross-covariance matrices are $\mathbf{P}_{ij} = \mathbb{E}[\zeta_i \zeta_j^{\top}]$ for $i, j \in \{1, \dots, n\}, i \neq j$. The composition \mathcal{X}_{com} is calculated as

$$\begin{aligned} \mathcal{X}_{\text{com}} &= \bar{\mathcal{X}}_1 \bar{\mathcal{X}}_2 \cdots \bar{\mathcal{X}}_{n-1} \bar{\mathcal{X}}_n \exp([\text{Ad}_{\bar{\mathcal{X}}_n^{-1} \cdots \bar{\mathcal{X}}_2^{-1}} \zeta_1]_{\wedge}) \\ &\quad \exp([\text{Ad}_{\bar{\mathcal{X}}_n^{-1} \cdots \bar{\mathcal{X}}_3^{-1}} \zeta_2]_{\wedge}) \cdots \exp([\text{Ad}_{\bar{\mathcal{X}}_n^{-1}} \zeta_{n-1}]_{\wedge}) \\ &\quad \exp([\zeta_n]_{\wedge}). \end{aligned} \quad (25)$$

We let $\mathcal{X}_{\text{com}} = \bar{\mathcal{X}}_{\text{com}} \exp([\zeta_{\text{com}}]_{\wedge})$ with $\zeta_{\text{com}} \sim \mathcal{N}(\mathbf{0}_{m \times 1}, \mathbf{P}_{\text{com}})$, then the mean $\bar{\mathcal{X}}_{\text{com}} \in \mathcal{G}_{\mathcal{X}}$ and its associated covariance matrix $\mathbf{P}_{\text{com}} \in \mathbb{R}^{m \times m}$ are

$$\bar{\mathcal{X}}_{\text{com}} = \bar{\mathcal{X}}_1 \bar{\mathcal{X}}_2 \cdots \bar{\mathcal{X}}_{n-1} \bar{\mathcal{X}}_n, \quad (26)$$

$$\mathbf{P}_{\text{com}} \approx \mathcal{M} \begin{bmatrix} \mathbf{P}_{nn} & \mathbf{P}_{nn-1} & \cdots & \mathbf{P}_{n1} \\ \mathbf{P}_{n-1n} & \mathbf{P}_{n-1n-1} & \cdots & \mathbf{P}_{n-11} \\ \vdots & \vdots & \ddots & \vdots \\ \mathbf{P}_{1n} & \mathbf{P}_{1n-1} & \cdots & \mathbf{P}_{11} \end{bmatrix} \mathcal{M}^{\top}, \quad (27)$$

where $\mathcal{M} = \text{diag}[\mathbf{I}_m \quad \text{Ad}_{\bar{\mathcal{X}}_n^{-1}} \quad \cdots \quad \text{Ad}_{\bar{\mathcal{X}}_n^{-1} \cdots \bar{\mathcal{X}}_2^{-1}}] \in \mathbb{R}^{mn \times mn}$. The proof is detailed in Appendix C.

C. Difference Operation

According to Fig.2-(c), for two stochastic members of $\mathcal{G}_{\mathcal{X}}$, $\mathcal{X}_1 = \bar{\mathcal{X}}_1 \exp([\zeta_1]_{\wedge})$ and $\mathcal{X}_2 = \bar{\mathcal{X}}_2 \exp([\zeta_2]_{\wedge})$, where $\zeta_i \sim \mathcal{N}(\mathbf{0}_{m \times 1}, \mathbf{P}_{ii})$, $i \in \{1, 2\}$, the difference is defined as

$$\mathcal{X}_{\text{dif}} = \mathcal{X}_1^{-1} \mathcal{X}_2. \quad (28)$$

This operation is a special case of composition when the first input is inverted. We let $\mathcal{X}_{\text{dif}} = \bar{\mathcal{X}}_{\text{dif}} \exp([\zeta_{\text{dif}}]_{\wedge})$ with $\zeta_{\text{dif}} \sim \mathcal{N}(\mathbf{0}_{m \times 1}, \mathbf{P}_{\text{dif}})$, then its mean $\bar{\mathcal{X}}_{\text{dif}}$ and covariance matrix \mathbf{P}_{dif} are (see Appendix D):

$$\bar{\mathcal{X}}_{\text{dif}} = \bar{\mathcal{X}}_1^{-1} \bar{\mathcal{X}}_2, \quad (29)$$

$$\begin{aligned} \mathbf{P}_{\text{dif}} &\approx \mathbf{P}_{22} - \mathbf{P}_{12}^{\top} \text{Ad}_{\bar{\mathcal{X}}_2^{-1}} \bar{\mathcal{X}}_1 - \text{Ad}_{\bar{\mathcal{X}}_2^{-1}} \bar{\mathcal{X}}_1 \mathbf{P}_{12} \\ &\quad + \text{Ad}_{\bar{\mathcal{X}}_2^{-1}} \bar{\mathcal{X}}_1 \mathbf{P}_{11} \text{Ad}_{\bar{\mathcal{X}}_2^{-1}}^{\top} \bar{\mathcal{X}}_1. \end{aligned} \quad (30)$$

D. Averaging Operation

Here, the averaging operation of stochastic members $\mathcal{X}_i = \bar{\mathcal{X}}_i \exp([\zeta_i]_{\wedge}) \in \mathcal{G}_{\mathcal{X}}$ with $\zeta_i \sim \mathcal{N}(\mathbf{0}_{m \times 1}, \mathbf{P}_{ii})$ for $i \in \{1, \dots, n\}$ is defined as

$$\mathcal{X}_{\text{avg}} = \mathcal{X}_1^{\alpha_1} \mathcal{X}_2^{\alpha_2} \cdots \mathcal{X}_n^{\alpha_n}, \quad (31)$$

where $\sum_{i=1}^n \alpha_i = 1$ and $\alpha_i \in [0, 1]$. We let $\mathcal{X}_{\text{avg}} = \bar{\mathcal{X}}_{\text{avg}} \exp([\zeta_{\text{avg}}]_{\wedge})$ with $\zeta_{\text{avg}} \sim \mathcal{N}(\mathbf{0}_{m \times 1}, \mathbf{P}_{\text{avg}})$, then the mean $\bar{\mathcal{X}}_{\text{avg}} \in \mathcal{G}_{\mathcal{X}}$ and covariance matrix $\mathbf{P}_{\text{avg}} \in \mathbb{R}^{m \times m}$ are

$$\bar{\mathcal{X}}_{\text{avg}} = \bar{\mathcal{X}}_1^{\alpha_1} \bar{\mathcal{X}}_2^{\alpha_2} \cdots \bar{\mathcal{X}}_{n-1}^{\alpha_{n-1}} \bar{\mathcal{X}}_n^{\alpha_n}, \quad (32)$$

$$\mathbf{P}_{\text{avg}} \approx \mathcal{M}_{\alpha} \begin{bmatrix} \mathbf{P}_{nn} & \mathbf{P}_{nn-1} & \cdots & \mathbf{P}_{n1} \\ \mathbf{P}_{n-1n} & \mathbf{P}_{n-1n-1} & \cdots & \mathbf{P}_{n-11} \\ \vdots & \vdots & \ddots & \vdots \\ \mathbf{P}_{1n} & \mathbf{P}_{1n-1} & \cdots & \mathbf{P}_{11} \end{bmatrix} \mathcal{M}_{\alpha}^{\top}, \quad (33)$$

where $\mathcal{M}_{\alpha} = \text{diag}[\alpha_n \mathbf{I}_m \quad \alpha_{n-1} \text{Ad}_{\bar{\mathcal{X}}_n^{-\alpha_n}} \quad \cdots \quad \alpha_1 \text{Ad}_{\bar{\mathcal{X}}_n^{-\alpha_n} \cdots \bar{\mathcal{X}}_2^{-\alpha_2}}]$. The proof follows a procedure similar to that of the composition in Appendix C, using the fact that $\mathcal{X}_i^{\alpha_i} = \bar{\mathcal{X}}_i^{\alpha_i} \exp(\alpha_i [\zeta_i]_{\wedge}) = \bar{\mathcal{X}}_i^{\alpha_i} \exp([\zeta_i^{\alpha_i}]_{\wedge})$ for the i^{th} member.

E. Fusion Operation

As illustrated in Fig.2-(d), the fusion problem aims to find an optimum consistent fused member $\mathcal{X}_{\text{fus}}^* = \bar{\mathcal{X}}_{\text{fus}}^* \exp([\zeta_{\text{fus}}^*]_{\wedge}) \in \mathcal{G}_{\mathcal{X}}$ with $\zeta_{\text{fus}}^* \sim \mathcal{N}(\mathbf{0}_{m \times 1}, \mathbf{P}_{\text{fus}})$ from a given set of n consistent and correlated stochastic members $\mathcal{X}_i = \bar{\mathcal{X}}_i \exp([\zeta_i]_{\wedge}) \in \mathcal{G}_{\mathcal{X}}$ with $\zeta_i \sim \mathcal{N}(\mathbf{0}_{m \times 1}, \mathbf{P}_{ii})$. The optimal fused member can be obtained from the following minimization problem [44]:

$$\mathcal{X}_{\text{fus}}^* = \arg \min_{\mathcal{X}_{\text{fus}}} \begin{bmatrix} \varepsilon_1 \\ \vdots \\ \varepsilon_n \end{bmatrix}^{\top} \begin{bmatrix} \mathbf{P}_{11} & \cdots & \mathbf{P}_{1n} \\ \vdots & \ddots & \vdots \\ \mathbf{P}_{1n}^{\top} & \cdots & \mathbf{P}_{nn} \end{bmatrix}^{-1} \begin{bmatrix} \varepsilon_1 \\ \vdots \\ \varepsilon_n \end{bmatrix}, \quad (34)$$

where the error between the i^{th} known member and the fused member is $\varepsilon_i = \left[\log(\bar{\mathcal{X}}_i^{-1} \mathcal{X}_{\text{fus}}^*) \right]_{\vee} \in \mathbb{R}^m$. The closed-form solution to this minimization problem is presented in [44]. For brevity, we only present the final derivation, as follows:

$$\bar{\mathcal{X}}_{\text{fus}} = \bar{\mathcal{X}}_s \exp([\bar{\zeta}_{\text{fus}}^*]_{\wedge}), \quad (35)$$

$$\mathbf{P}_{\text{fus}} = \mathcal{J}_r(\bar{\zeta}_{\text{fus}}^*) \mathbf{P}_{\zeta \zeta}^* \mathcal{J}_r^{\top}(\bar{\zeta}_{\text{fus}}^*). \quad (36)$$

Here, $\bar{\mathcal{X}}_s$ is an arbitrary reference member and

$$\begin{aligned} \bar{\zeta}_{\text{fus}}^* = & - \left(\sum_{i=1}^N \sum_{j=1}^N \mathcal{J}_r^{-\top}(\zeta_j) \mathbf{G}_{ij}^\top \mathcal{J}_r^{-1}(\zeta_i) \right. \\ & \left. + \mathcal{J}_r^{-\top}(\zeta_i) \mathbf{G}_{ij} \mathcal{J}_r^{-1}(\zeta_j) \right)^{-1} \\ & \sum_{i=1}^N \sum_{j=1}^N \mathcal{J}_r^{-\top}(\zeta_j) \mathbf{G}_{ij}^\top \zeta_i + \mathcal{J}_r^{-\top}(\zeta_i) \mathbf{G}_{ij} \zeta_j, \end{aligned} \quad (37)$$

$$\begin{aligned} \mathbf{P}_{\zeta\zeta}^* = & \left(\sum_{i=1}^N \sum_{j=1}^N \mathcal{J}_r^{-\top}(\zeta_j) \mathbf{G}_{ij}^\top \mathcal{J}_r^{-1}(\zeta_i) \right. \\ & \left. + \mathcal{J}_r^{-\top}(\zeta_i) \mathbf{G}_{ij} \mathcal{J}_r^{-1}(\zeta_j) \right)^{-1}, \end{aligned} \quad (38)$$

where $\zeta_i = [\log(\bar{\mathcal{X}}_i^{-1} \bar{\mathcal{X}}_s)]_{\vee}$ and

$$\mathbf{G} = \begin{bmatrix} \mathbf{P}_{11} & \cdots & \mathbf{P}_{1n} \\ \vdots & \ddots & \vdots \\ \mathbf{P}_{1n}^\top & \cdots & \mathbf{P}_{nn} \end{bmatrix}^{-1} = \begin{bmatrix} \mathbf{G}_{11} & \cdots & \mathbf{G}_{1N} \\ \vdots & \ddots & \vdots \\ \mathbf{G}_{N1} & \cdots & \mathbf{G}_{NN} \end{bmatrix} \in \mathbb{R}^{mn \times mn}.$$

Furthermore, in an EKF-based estimation framework, the cross-covariance matrix between correlated estimates is calculated from the following recursion [44]:

$$\begin{aligned} \mathbf{P}_{ij(k|k)} = & (\mathbf{I}_m - \mathbf{K}_i(k) \mathcal{H}_i(k)) \left(\mathcal{F}_{i(k-1)} \mathbf{P}_{ij(k-1|k-1)} \mathcal{F}_j^\top(k-1) \right. \\ & \left. + \mathcal{J}_r(\bar{\mathbf{f}}_i(k-1)) \mathbf{Q}(k-1) \mathcal{J}_r^\top(\bar{\mathbf{f}}_j(k-1)) \right) (\mathbf{I}_m - \mathbf{K}_j(k) \mathcal{H}_j(k))^\top. \end{aligned}$$

F. Constrained Fusion

In some frameworks, the estimated member is required to lie on a constrained surface. In this section, we propose a method to project the unconstrained fused estimate $\bar{\mathcal{X}}_u = \bar{\mathcal{X}}_{\text{fus}}^*$ onto a constraint space defined by $\{\bar{\mathcal{X}}_c \in \mathcal{G}_{\mathcal{X}} | \mathbf{g}(\bar{\mathcal{X}}_c) = \mathbf{D}\}$. Here, $\bar{\mathcal{X}}_c$ is the constrained estimate, $\mathbf{g} : \mathcal{G}_{\mathcal{X}} \rightarrow \mathcal{G}_{\mathcal{X}_c}$ is a map to the constraint matrix Lie group $\mathcal{G}_{\mathcal{X}_c}$ with the dimension $r \leq m$, and $\mathbf{D} \in \mathcal{G}_{\mathcal{X}_c}$ is a constant member. To this end, we solve the following minimization problem:

$$\begin{aligned} \bar{\mathcal{X}}_c^* = & \arg \min_{\bar{\mathcal{X}}_c} ([\log(\bar{\mathcal{X}}_u^{-1} \bar{\mathcal{X}}_c)]_{\vee})^\top \mathbf{W}_c ([\log(\bar{\mathcal{X}}_u^{-1} \bar{\mathcal{X}}_c)]_{\vee}), \\ \mathbf{D} = & \mathbf{g}(\bar{\mathcal{X}}_c), \end{aligned} \quad (39)$$

where, $\mathbf{W}_c \in \mathbb{R}^{m \times m}$ is any symmetric positive definite weighting matrix. To solve this problem, we define a reference member $\bar{\mathcal{X}}_s$ and write $\bar{\mathcal{X}}_c = \bar{\mathcal{X}}_s \exp([\zeta_c]_{\wedge})$. We then find the optimum value for the unknown error ζ_c on Lie algebra $\mathfrak{g}_{\mathcal{X}}$ using the known vector $\zeta_u = [\log(\bar{\mathcal{X}}_u^{-1} \bar{\mathcal{X}}_s)]_{\vee}$. Assuming ζ_c is small and using (10), the minimization problem reduces to

$$\begin{aligned} \zeta_c^* = & \arg \min_{\zeta_c} (\zeta_u + \mathcal{J}_r^{-1}(\zeta_u) \zeta_c)^\top \mathbf{W}_c (\zeta_u + \mathcal{J}_r^{-1}(\zeta_u) \zeta_c), \\ \tilde{\mathbf{d}} = & \tilde{\mathbf{g}}(\zeta_c), \end{aligned} \quad (40)$$

where, $\tilde{\mathbf{d}} = [\log(\mathbf{D})]_{\vee}$ and $\tilde{\mathbf{g}}(\zeta_c) = [\log(\mathbf{g}(\bar{\mathcal{X}}_s \exp([\zeta_c]_{\wedge})))]_{\vee}$ are vectors in \mathbb{R}^r , $r \leq m$. The constrained minimization problem (40) can be solved using the Lagrange multiplier method [71]. The Lagrangian is defined as:

$$\mathcal{L} = (\zeta_u + \mathcal{J}_r^{-1}(\zeta_u) \zeta_c)^\top \mathbf{W}_c (\zeta_u + \mathcal{J}_r^{-1}(\zeta_u) \zeta_c) + 2\lambda^\top (\tilde{\mathbf{g}}(\zeta_c) - \tilde{\mathbf{d}}), \quad (41)$$

where, $\lambda \in \mathbb{R}^r$ is the vector of Lagrange multipliers. We then find the necessary conditions for the minimum, which are obtained by solving the following set of algebraic equations:

$$\begin{aligned} \frac{\partial \mathcal{L}}{\partial \zeta_c} = & \mathcal{J}_r^{-\top}(\zeta_u) \mathbf{W}_c (\zeta_u + \mathcal{J}_r^{-1}(\zeta_u) \zeta_c) + \frac{\partial \tilde{\mathbf{g}}^\top}{\partial \zeta_c}(\zeta_c) \lambda = \mathbf{0}_{m \times 1}, \\ \frac{\partial \mathcal{L}}{\partial \lambda} = & \tilde{\mathbf{g}}(\zeta_c) - \tilde{\mathbf{d}} = \mathbf{0}_{r \times 1}. \end{aligned}$$

Here, we solve this system for the specific case where the constraint function is linear in ζ_c , i.e., $\tilde{\mathbf{g}}(\zeta_c) = \mathbf{\Gamma} \zeta_c$ where $\mathbf{\Gamma} \in \mathbb{R}^{r \times m}$, $r < m$. We also assume the constraints are linearly independent, i.e., $\mathbf{\Gamma}$ has rank r . In this case the closed form solution is

$$\begin{aligned} \zeta_c^* = & \mathfrak{J} \left[\left(\mathbf{\Gamma}^\top (\mathbf{\Gamma} \mathfrak{J} \mathbf{\Gamma}^\top)^{-1} \mathbf{\Gamma} \mathfrak{J} \mathcal{J}_r^{-\top}(\zeta_u) \mathbf{W}_c \right. \right. \\ & \left. \left. - \mathcal{J}_r^{-\top}(\zeta_u) \mathbf{W}_c \right) \zeta_u + \mathbf{\Gamma}^\top (\mathbf{\Gamma} \mathfrak{J} \mathbf{\Gamma}^\top)^{-1} \tilde{\mathbf{d}} \right], \end{aligned} \quad (42)$$

where, $\mathfrak{J} = (\mathcal{J}_r^{-\top}(\zeta_u) \mathbf{W}_c \mathcal{J}_r^{-1}(\zeta_u))^{-1}$. Note that if $r = m$, then (42) reduces to $\zeta_c^* = \mathbf{\Gamma}^{-1} \tilde{\mathbf{d}}$. The derivation process of (42) is detailed in Appendix E.

IV. LOCALIZATION FRAMEWORK

In this section, we use the stochastic operations defined in Section III to propose a collaborative localization system for a group of n robots operating under the following conditions:

- The robots operate in a GPS-denied indoor environment and they are equipped with inertial sensors (e.g., IMU), velocity sensors (e.g., wheel encoders), and pose estimation modules (e.g., marker-based).
- They are equipped with communication devices such as WiFi that enable inter-robot communication.
- The robots are classified into three types: leader, which obtains global pose information from stationary markers; follower type 1, which communicates with the leader and obtains relative pose information from the leader's mobile markers; and follower type 2, which communicates with a follower (either type 1 or 2) and obtains relative pose information from its mobile markers. The follower type is dynamic, i.e., a robot may be follower type 1 or 2, depending on whether a leader is in its field of view.
- Each robot runs a local EKF, in which inertial sensor measurements are used for prediction, while velocity and pose measurements are used for update.

A. Inertial Prediction

Given an inertial sensor such as IMU within a body coordinate frame $\{B\}$ moving relative to the robot's global coordinate frame $\{O\}$, and assuming its readings are solely affected by noise and bias errors, the measured angular velocity $\tilde{\omega}^{OB}$ (from gyros of IMU) and acceleration $\tilde{\mathbf{a}}_B^O$ (from accelerometers of IMU) are

$$\tilde{\omega}^{OB} = \omega^{OB} + \mathbf{b}_g + \mathbf{w}_g, \quad (43)$$

$$\tilde{\mathbf{a}}_B^O = \mathbf{a}_B^O + \mathbf{b}_a + \mathbf{w}_a. \quad (44)$$

Here, $\omega^{OB} \in \mathbb{R}^3$ denotes the true angular velocity of frame $\{B\}$ relative to frame $\{O\}$, while $\mathbf{a}_B^O \in \mathbb{R}^3$ is the true

The leader robot's global coordinate frame, $\{O_l\}$, serves as the reference for the robot's inertial and velocity sensors (IMU and WO), as conventionally set on the onboard computer. The robot's body frame is denoted as $\{B_l\}$ while the camera coordinate frame on the leader is $\{C_l\}$. Finally, $\{M_l\}$ serves as the landmark's coordinate frame. To follow the ground truth motion of the robots in Section V, we also define the coordinate frame of a motion tracker system, denoted as $\{W\}$, which has a fixed offset relative to $\{U\}$.

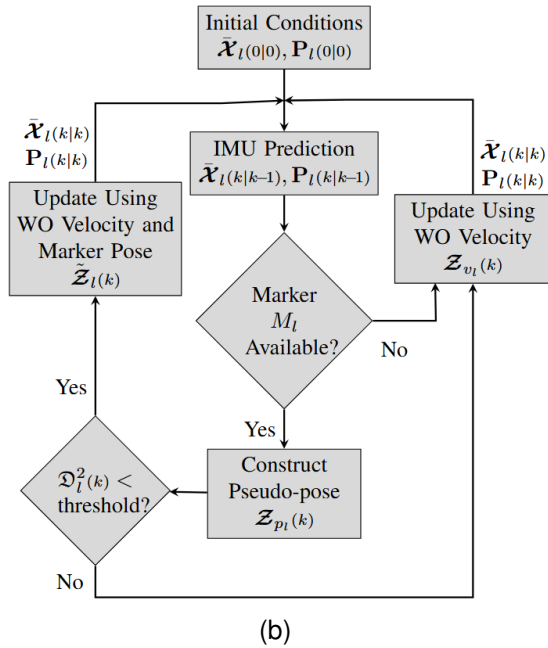
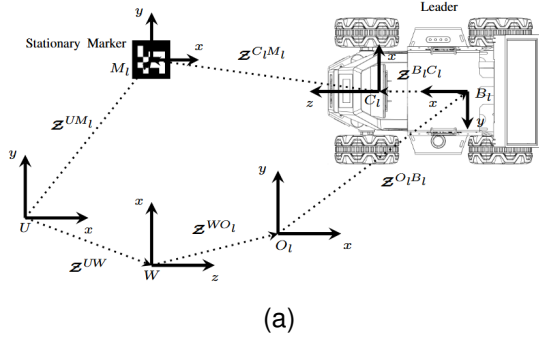


Fig. 3. A leader robot's (a) coordinate frames, and (b) estimation framework.

To determine a leader's pseudo-pose in the form of $\mathcal{Z}_{p_l} := \mathcal{Z}^{O_l B_l} = \begin{bmatrix} \mathcal{R}_p^{O_l B_l} & \mathbf{p}_{B_l p}^{O_l} \\ \mathbf{0}_{1 \times 3} & 1 \end{bmatrix} \in \mathbb{SE}(3)$, we use the relation:

$$\mathcal{Z}^{O_l B_l} = (\mathcal{Z}^{UW} \mathcal{Z}^{WO_l})^{-1} \mathcal{Z}^{UM_l} (\mathcal{Z}^{B_l C_l} \mathcal{Z}^{C_l M_l})^{-1}, \quad (55)$$

where throughout this paper, we denote the relative pose between two generic frames $\{X\}$ and $\{Y\}$ by $\mathcal{Z}^{XY} = \begin{bmatrix} \mathcal{R}^{XY} & \mathbf{p}_Y^X \\ \mathbf{0}_{1 \times 3} & 1 \end{bmatrix} \in \mathbb{SE}(3)$. The members \mathcal{Z}^{UW} , \mathcal{Z}^{WO_l} , \mathcal{Z}^{UM_l} and $\mathcal{Z}^{B_l C_l}$ are known and deterministic, while $\mathcal{Z}^{C_l M_l}$ represents the stochastic member provided by camera measurements. These measurements are corrupted by noise and we assume their associated uncertainty follows a zero-mean Gaussian process. Thus, the leader's camera measurements are $\mathcal{Z}^{C_l M_l} =$

$\bar{\mathcal{Z}}^{C_l M_l} \exp(\left[\zeta_{M_l}^{C_l} \right]_{\wedge})$ with $\zeta_{M_l}^{C_l} \sim \mathcal{N}(\mathbf{0}_{1 \times 6}, \mathbf{R}_{m_l})$ and noise covariance $\mathbf{R}_{m_l} \in \mathbb{R}^{6 \times 6}$. We then apply the operations developed in Section III to derive the mean and covariance matrix of \mathcal{Z}_{p_l} as follows:

$$\bar{\mathcal{Z}}_{p_l} = (\mathcal{Z}^{UW} \mathcal{Z}^{WO_l})^{-1} \mathcal{Z}^{UM_l} (\mathcal{Z}^{B_l C_l} \bar{\mathcal{Z}}^{C_l M_l})^{-1}, \quad (56)$$

$$\mathbf{R}_{p_l} \approx \mathbf{Ad}_{\mathcal{Z}^{B_l C_l}} \mathbf{Ad}_{\bar{\mathcal{Z}}^{C_l M_l}} \mathbf{R}_{m_l} \mathbf{Ad}_{\bar{\mathcal{Z}}^{C_l M_l}}^{\top} \mathbf{Ad}_{\mathcal{Z}^{B_l C_l}}^{\top}. \quad (57)$$

When both velocity measurements $\mathcal{Z}_{v_l}(k) = \mathbf{v}_{B_l v}^{O_l}(k)$ and pseudo-pose measurements $\mathcal{Z}_{p_l}(k)$ are available and reliable (refer to Section IV-D for sensor fault detection), the update is done on $\mathcal{G}_{\mathcal{Z}} := \mathbb{SE}(3) \times \mathbb{R}^3$ whose members are in the following form:

$$\tilde{\mathcal{Z}}_l(k) = \begin{bmatrix} \mathcal{R}_p^{O_l B_l}(k) & \mathbf{p}_{B_l p}^{O_l}(k) & & \\ \mathbf{0}_{1 \times 3} & 1 & & \\ & & \mathbf{0}_4 & \\ & & & \begin{bmatrix} \mathbf{I}_3 & \mathbf{v}_{B_l v}^{O_l}(k) \\ \mathbf{0}_{1 \times 3} & 1 \end{bmatrix} \end{bmatrix} \in \mathbb{R}^{8 \times 8}.$$

Details of the matrix Lie group $\mathcal{G}_{\mathcal{Z}}$ are provided in Appendix A. Thus, the measurement model is as follows:

$$\mathcal{Z}_l(k) = \begin{bmatrix} \mathcal{R}^{O_l B_l}(k) & \mathbf{p}_{B_l p}^{O_l}(k) & & \\ \mathbf{0}_{1 \times 3} & 1 & & \\ & & \mathbf{0}_4 & \\ & & & \begin{bmatrix} \mathbf{I}_3 & \mathcal{R}^{O_l B_l \top}(k) \mathbf{v}_{B_l v}^{O_l}(k) \\ \mathbf{0}_{1 \times 3} & 1 \end{bmatrix} \end{bmatrix} \exp([\mathbf{m}_l(k)]_{\wedge}),$$

where, $\mathbf{m}_l(k)$ is a zero-mean noise vector with the noise covariance matrix $\mathbf{R}_l = \text{diag}([\mathbf{R}_{p_l}, \epsilon \mathbf{I}_3, \mathbf{R}_{v_l}]) \in \mathbb{R}^{12 \times 12}$, and $\epsilon \ll 1$ to avoid inversion of zero.

2) *Pose Update for Follower Type 1*: Here, we introduce additional coordinate frames for the follower type 1 robot including the global frame $\{O_{f_1}\}$, body frame $\{B_{f_1}\}$, camera frame $\{C_{f_1}\}$, and mobile landmark (fiducial marker) frame on the leader and observed by the follower type 1 $\{M_{f_1}\}$. As shown in Fig.4-(a), there are two paths to construct $\mathcal{Z}^{O_{f_1} B_{f_1}}$. The first approach relies on stochastic members $\mathcal{Z}^{C_{f_1} M_{f_1}}$ and $\mathcal{Z}^{C_l M_l}$ —the raw observations of the mobile and stationary markers M_{f_1} and M_l , respectively. The second path relies on the estimated pose of the leader robot and the follower's relative pose observation of the mobile marker M_{f_1} , i.e.,

$$\mathcal{Z}^{O_{f_1} B_{f_1}} = (\mathcal{Z}^{WO_{f_1}})^{-1} \mathcal{Z}^{WO_l} \mathcal{Z}^{O_l B_l} (\mathcal{Z}^{B_{f_1} C_{f_1}} \mathcal{Z}^{C_{f_1} M_{f_1}} \mathcal{Z}^{M_{f_1} B_l})^{-1},$$

where we use $\mathcal{Z}^{O_l B_l} = \bar{\mathcal{X}}_l^{\mathbb{SE}(3)} \exp(\left[\zeta_l^{\mathbb{SE}(3)} \right]_{\wedge})$ with $\zeta_l^{\mathbb{SE}(3)} \sim \mathcal{N}(\mathbf{0}_{1 \times 6}, \mathbf{P}_l^{\mathbb{SE}(3)})$ and $\mathbf{P}_l^{\mathbb{SE}(3)} \in \mathbb{R}^{6 \times 6}$. Note that $\bar{\mathcal{X}}_l^{\mathbb{SE}(3)}$ is the pose part of the current estimated state of the leader in its local EKF and $\zeta_l^{\mathbb{SE}(3)}$ is its associated uncertainty. This method's advantage lies in using the leader robot's estimated pose, which is available at a higher frequency and can be transmitted more quickly than raw marker measurements. We then let $\mathcal{Z}^{C_{f_1} M_{f_1}} = \bar{\mathcal{Z}}^{C_{f_1} M_{f_1}} \exp(\left[\zeta_{M_{f_1}}^{C_{f_1}} \right]_{\wedge})$ with $\zeta_{M_{f_1}}^{C_{f_1}} \sim \mathcal{N}(\mathbf{0}_{1 \times 6}, \mathbf{R}_{m_{f_1}})$ with $\mathbf{R}_{m_{f_1}} \in \mathbb{R}^{6 \times 6}$ to obtain the mean and covariance of the stochastic member $\mathcal{Z}_{p_{f_1}} := \mathcal{Z}^{O_{f_1} B_{f_1}} = \begin{bmatrix} \mathcal{R}_p^{O_{f_1} B_{f_1}} & \mathbf{p}_{B_{f_1} p}^{O_{f_1}} \\ \mathbf{0}_{1 \times 3} & 1 \end{bmatrix} \in \mathbb{SE}(3)$ as follows:

$$\bar{\mathcal{Z}}_{p_{f_1}} = (\mathcal{Z}^{WO_{f_1}})^{-1} \mathcal{Z}^{WO_l} \bar{\mathcal{X}}_l^{\mathbb{SE}(3)} (\mathcal{Z}^{B_{f_1} C_{f_1}} \bar{\mathcal{Z}}^{C_{f_1} M_{f_1}} \mathcal{Z}^{M_{f_1} B_l})^{-1},$$

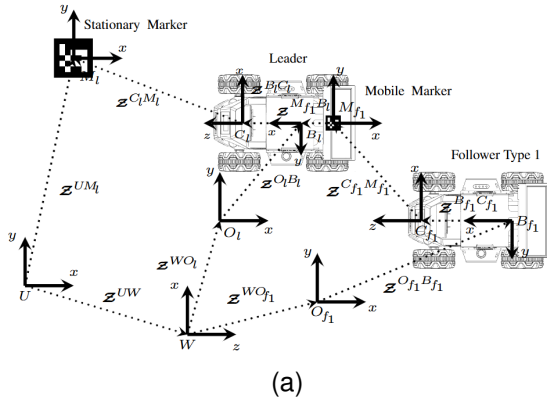
$$\mathbf{R}_{p_{f_1}} \approx \mathbf{Ad}_{\mathcal{Z}^{B_{f_1} C_{f_1}}} \mathbf{Ad}_{\bar{\mathcal{Z}}^{C_{f_1} M_{f_1}}} \mathbf{R}_{m_{f_1}} \mathbf{Ad}_{\bar{\mathcal{Z}}^{C_{f_1} M_{f_1}}}^{\top} \mathbf{Ad}_{\mathcal{Z}^{B_{f_1} C_{f_1}}}^{\top} +$$

$$\mathbf{Ad}_{\mathcal{Z}^{B_{f_1} C_{f_1}}} \bar{\mathcal{Z}}^{C_{f_1} M_{f_1}} \bar{\mathcal{Z}}^{M_{f_1} B_l} \mathbf{P}_l^{\mathbb{SE}(3)} \mathbf{Ad}_{\bar{\mathcal{Z}}^{C_{f_1} M_{f_1}}}^{\top} \mathbf{Ad}_{\mathcal{Z}^{B_{f_1} C_{f_1}}}^{\top} \bar{\mathcal{Z}}^{M_{f_1} B_l}.$$

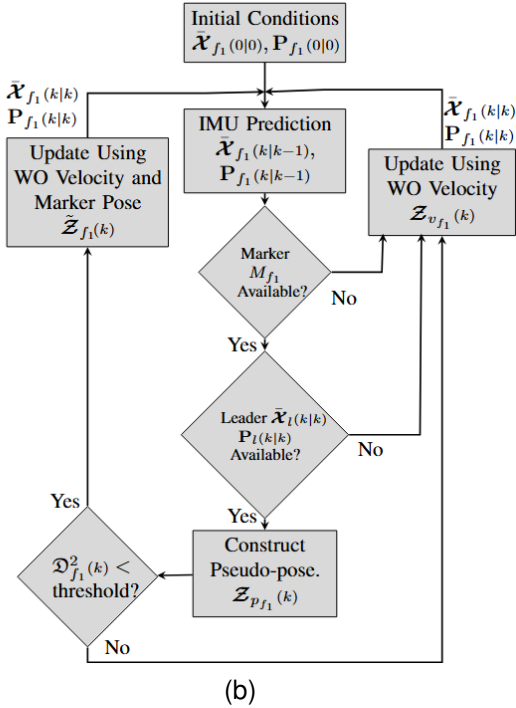
The next step updates the follower robot's predictions using its velocity measurements $\mathcal{Z}_{v_{f_1}}(k) = \mathbf{v}_{B_{f_1}^i}^{O_{f_1}}(k)$ and the constructed pseudo-pose measurements $\mathcal{Z}_{p_{f_1}}$ on the manifold $\mathcal{G}_{\mathcal{Z}} := \text{SE}(3) \times \mathbb{R}^3$ provided that the constructed pseudo-poses are reliable (refer to Section IV-D). Thus, the measurement member is in the following form:

$$\tilde{\mathcal{Z}}_{f_1}(k) = \begin{bmatrix} \mathcal{R}_p^{O_{f_1}B_{f_1}}(k) & \mathbf{P}_{B_{f_1}^i}^{O_{f_1}}(k) & & \mathbf{0}_4 \\ \mathbf{0}_{1 \times 3} & 1 & & \\ & & \mathbf{0}_4 & \\ & & & \begin{bmatrix} \mathbf{I}_3 & \mathbf{v}_{B_{f_1}^i}^{O_{f_1}}(k) \\ \mathbf{0}_{1 \times 3} & 1 \end{bmatrix} \end{bmatrix} \in \mathbb{R}^{8 \times 8}.$$

The covariance matrix of the measurement $\tilde{\mathcal{Z}}_{f_1}$ is obtained from $\mathbf{R}_{f_1} = \text{diag}([\mathbf{R}_{p_{f_1}}, \epsilon \mathbf{I}_3, \mathbf{R}_{v_{f_1}}]) \in \mathbb{R}^{12 \times 12}$.



(a)



(b)

Fig. 4. Follower type 1 robot, (a) coordinate frames, (b) estimation framework.

3) *Pose Update for Follower Type 2*: Here, we develop the pseudo-pose of a follower robot type 2 with robot global frame $\{O_{f_2}\}$, camera frame $\{C_{f_2}\}$ and body frame $\{B_{f_2}\}$ based on its observations of a mobile landmark (fiducial marker) with

coordinate frame $\{M_{f_2}\}$ installed on a neighboring follower robot, as well as the estimates from a type i (can be 1 or 2) neighboring robot with robot and body frames $\{O_{f_i}\}$ and $\{B_{f_i}\}$. As illustrated in Fig.5-(a) the following relation holds:

$$\mathcal{Z}_{p_{f_2}} := \mathcal{Z}_i^{O_{f_2}B_{f_2}} = (\mathcal{Z}^{WO_{f_2}})^{-1} \mathcal{Z}^{WO_{f_i}} \mathcal{Z}^{O_{f_i}B_{f_i}} (\mathcal{Z}^{B_{f_2}C_{f_2}} \mathcal{Z}^{C_{f_2}M_{f_2}} \mathcal{Z}^{M_{f_2}B_{f_i}})^{-1}.$$

Applying the inverse and composition methods, the mean and covariance of the pseudo-pose $\mathcal{Z}_{p_{f_2}}$ are

$$\bar{\mathcal{Z}}_{p_{f_2}} = (\mathcal{Z}^{WO_{f_2}})^{-1} \mathcal{Z}^{WO_{f_i}} \bar{\mathcal{X}}_{f_i}^{\text{SE}(3)} (\mathcal{Z}^{B_{f_2}C_{f_2}} \bar{\mathcal{Z}}^{C_{f_2}M_{f_2}} \mathcal{Z}^{M_{f_2}B_{f_i}})^{-1},$$

$$\mathbf{R}_{p_{f_2}} \approx \text{Ad}_{\mathcal{Z}^{B_{f_2}C_{f_2}}} \text{Ad}_{\bar{\mathcal{Z}}^{C_{f_2}M_{f_2}}} \mathbf{R}_{m_{f_2}} \text{Ad}_{\mathcal{Z}^{C_{f_2}M_{f_2}}}^\top \text{Ad}_{\mathcal{Z}^{M_{f_2}B_{f_i}}}^\top +$$

$$\text{Ad}_{\mathcal{Z}^{B_{f_2}C_{f_2}}} \bar{\mathcal{Z}}^{C_{f_2}M_{f_2}} \mathcal{Z}^{M_{f_2}B_{f_i}} \mathbf{P}_{f_i}^{\text{SE}(3)} \text{Ad}_{\mathcal{Z}^{B_{f_2}C_{f_2}}}^\top \text{Ad}_{\mathcal{Z}^{C_{f_2}M_{f_2}}}^\top \mathcal{Z}^{C_{f_2}M_{f_2}} \mathcal{Z}^{M_{f_2}B_{f_i}},$$

where $\mathcal{Z}^{O_{f_i}B_{f_i}} = \bar{\mathcal{X}}_{f_i}^{\text{SE}(3)} \exp(\zeta_{f_i}^{\text{SE}(3)})$ with $\zeta_{f_i}^{\text{SE}(3)} \sim \mathcal{N}(\mathbf{0}_{1 \times 6}, \mathbf{P}_{f_i}^{\text{SE}(3)})$ and $\mathcal{Z}^{C_{f_2}M_{f_2}} = \bar{\mathcal{Z}}^{C_{f_2}M_{f_2}} \exp(\zeta_{M_{f_2}}^{C_{f_2}})$ with $\zeta_{M_{f_2}}^{C_{f_2}} \sim \mathcal{N}(\mathbf{0}_{1 \times 6}, \mathbf{R}_{m_{f_2}})$.

We let $\mathcal{Z}_{p_{f_2}} = \begin{bmatrix} \mathcal{R}_p^{O_{f_2}B_{f_2}} & \mathbf{P}_{B_{f_2}^i}^{O_{f_2}} \\ \mathbf{0}_{1 \times 3} & 1 \end{bmatrix}$, then the measurement matrix for a follower type 2 from observing the follower type i is as follows:

$$\tilde{\mathcal{Z}}_{f_2}(k) = \begin{bmatrix} \mathcal{R}_p^{O_{f_2}B_{f_2}}(k) & \mathbf{P}_{B_{f_2}^i}^{O_{f_2}}(k) & & \mathbf{0}_4 \\ \mathbf{0}_{1 \times 3} & 1 & & \\ & & \mathbf{0}_4 & \\ & & & \begin{bmatrix} \mathbf{I}_3 & \mathbf{v}_{B_{f_2}^i}^{O_{f_2}}(k) \\ \mathbf{0}_{1 \times 3} & 1 \end{bmatrix} \end{bmatrix} \in \mathbb{R}^{8 \times 8},$$

with the covariance matrix of $\mathbf{R}_{f_2} = \text{diag}([\mathbf{R}_{p_{f_2}}, \epsilon \mathbf{I}_3, \mathbf{R}_{v_{f_2}}]) \in \mathbb{R}^{12 \times 12}$. The update is done if the constructed pseudo-poses are reliable (Section IV-D).

D. Fault Detection (FD)

To diagnose faults in measurements, a statistical index known as the Mahalanobis distance is used [72]. The Mahalanobis distance quantifies the goodness-of-fit between observed measurements $\tilde{\mathcal{Z}}(k)$ and theoretical expected measurements $\bar{\mathcal{Z}}(k) = \mathbf{h}(\bar{\mathcal{X}}(k|k-1))$. This index and its squared have been widely used in the literature for sensor fault/anomaly diagnosis [73]. Here, we use the squared Mahalanobis distance and define it for the system (11)-(12) as

$$\mathcal{D}^2(k) = \boldsymbol{\nu}^\top(k) (\mathcal{H}(k) \mathbf{P}(k|k-1) \mathcal{H}^\top(k) + \mathbf{R}(k))^{-1} \boldsymbol{\nu}(k), \quad (58)$$

where, the innovation vector on matrix Lie groups is

$$\boldsymbol{\nu}(k) = [\log(\mathbf{h}^{-1}(\bar{\mathcal{X}}(k|k-1)) \mathcal{Z}(k))]_{\vee}. \quad (59)$$

To filter the faulty measurements, the update step of the EKF is performed when a new measurement $\mathcal{Z}(k)$ is received and the calculated value of $\mathcal{D}^2(k)$ is found to be below a pre-defined threshold. The Mahalanobis index $\mathcal{D}_l^2(k)$ for a leader robot is calculated when stationary marker measurements are available. For the follower type 1, when both mobile marker measurements and estimates of the leader robot are available the index $\mathcal{D}_{f_1}^2(k)$ is calculated. Finally, in the follower type 2 framework, when mobile marker measurements and the pose estimate of the i^{th} follower robot are available the index

2) *IMU Calibration*: MPU-6050 is an integrated 6-axis IMU combining a 3-axis gyroscope, a 3-axis accelerometer, and a digital motion processor. Since the IMU measures normal forces, it is necessary to account for local gravity to correct the acceleration along the axis perpendicular to the ground. At the test site, with an elevation of 70 *m* and a latitude of $45.424721^\circ N$, the local gravity is $9.80637 \frac{m}{s^2}$. The IMU calibration involves placing the robot in a stable position on a flat surface and recording raw data for 100 seconds. The offsets for each axis are then computed as the average sensor readings.

3) *Aruco Marker Pose Estimation*: Using the ROS package [77], the algorithm extracts ArUco marker corners, identifies their unique IDs, and calculates the marker's 3-D pose relative to the camera frame. In our experiments, we utilized the 5×5 original ArUco dictionary. An ArUco with size 36 *cm* and ID=25 was used for the stationary marker, while mobile marker were 8.5 *cm* with ID=102 and ID=104.

C. Setup Refinement

To investigate the effects of various factors and refine the setup, we conducted a series of experiments. A robot, equipped with an upward-facing camera, follows a circular path around a stationary marker mounted on the ceiling and the pseudo-pose measurements are constructed based on the model described in Section IV-C. We examined the effects of lighting conditions by comparing results under full and reduced lighting, the impact of marker size by testing three marker dimensions (17 *cm*, 36 *cm*, and 56 *cm*), and the influence of the robot's forward speed using three speeds (5 *cm/s*, 10 *cm/s*, and 50 *cm/s*).

The results illustrated in Fig.7 highlight three key points. First, by comparing Fig.7-(a) and Fig.7-(b), we observe that when the lights are fully on, the increased reflections and glare on the camera lens leads to noisier measurements. This experiment highlights the importance of maintaining a uniform lighting environment. Second, comparing the results in Fig.7-(a), (c), and (d) show that the size of the ArUco marker significantly affects the performance. When the marker size is 17 *cm*, the system performs poorly, but as the marker size increases, less noisy measurements are obtained. Finally, a comparison of Fig.7-(a), (e), and (f) shows that at higher speeds, the robot's smoother motion helps reduce the effects of small distortions and environmental variations, thereby improving pose estimation performance. However, it is important to note that excessively high speeds may eventually exceed the system's capacity to detect the marker. In our setup, due to space limitations, as well as considerations regarding the motion tracker, safety, and placement of the ArUco marker, we used a 36 *cm* ArUco, set the robot speed to 10 *cm/s*, and keep the lights on for the remaining experiments.

D. Localization Results

1) *Leader Robot Localization Results*: Here, we investigate the localization of a leader robot subjected to various trajectories, including circular motion, cornering motions, and traverse over uneven terrain created by square foam mats placed

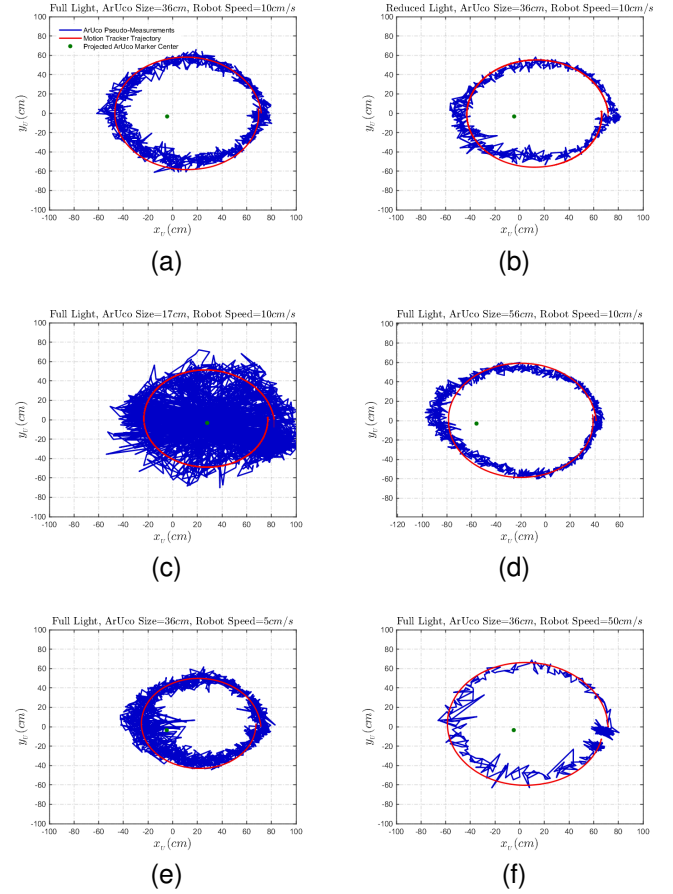


Fig. 7. Effects of lighting conditions, marker size, and robot speed on the accuracy of ArUco pseudo-pose measurements.

along the path (See Fig.6-(c)). In the experiments, sensor fusion is performed with $\mathbf{Q}_g = \mathbf{Q}_{b_g} = 10^{-6} \mathbf{I}_3 \text{ rad}^2/s^2$, $\mathbf{Q}_a = \mathbf{Q}_{b_a} = \mathbf{I}_3 \text{ m}^2/s^4$, $\mathbf{R}_{v_l} = 0.00015 \mathbf{I}_3 \text{ m}^2/s^2$, $\mathbf{R}_{m_l} = \text{diag}([0.0075 \mathbf{I}_3 \text{ rad}^2, 0.005 \mathbf{I}_3 \text{ m}^2])$, and $\mathbf{P}(0|0) = 10^{-2} \mathbf{I}_{18}$. Moreover, the threshold in all cases is set to 40. The results are presented in Fig.8, from which we draw the following conclusions. The IMU trajectory fails quickly in all scenarios due to the robot being equipped with a low-cost IMU. A comparison between Fig.8-(a) and Fig.8-(b) reveals that WO fails when the robot attempts to turn, with the failure being particularly pronounced during the circular motion. Although the fusion of IMU and WO yields reasonable results, notable errors persist, underscoring the importance of incorporating more accurate measurements from the ArUco markers. Furthermore, when the robot turns around the ceiling-mounted lights during the circular motion (Fig.8-(a)) or traverses the square foam mats (Fig. 8-(d)), ArUco pseudo-pose measurements become subject to significant noise. In these cases, the inclusion of the FD module effectively removes outliers. Thus, the fusion of IMU, WO, ArUco pseudo-poses, and FD more accurately captures the ground truth trajectory across all three types of motion.

Initial value of the covariance matrix is another factor impacting the EKF performance. Fig 9 shows the captured trajectory for the IMU/WO and IMU/WO/ArUco/FD filters

with different initial covariance values. The results verify that when the initial covariance is too low or too high, the IMU/WO trajectory exhibits significant deviations, while the IMU/WO/ArUco/FD filter shows little to no sensitivity to changes in $P(0|0) = P_0$.

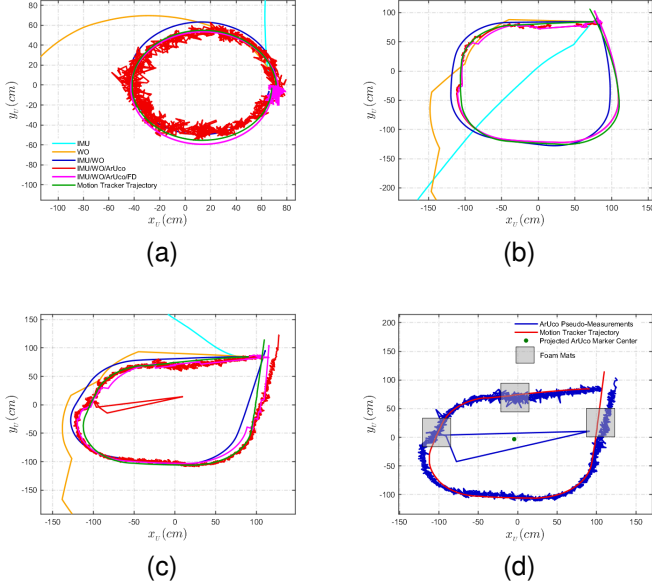


Fig. 8. Leader localization performance; (a) circular motion, (b) cornering motion, (c) uneven motion, and (d) ArUco measurements of uneven motion

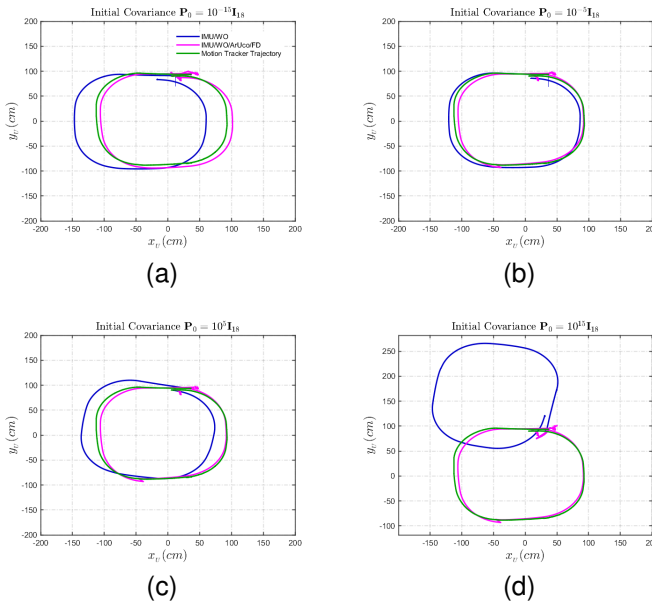


Fig. 9. Effect of Initial Covariance P_0 on Localization Performance

2) *Follower Type 1 Localization Results:* In this experiment, the leader robot is equipped with an upward-facing camera that captures pose measurements from a stationary 36 cm ArUco marker mounted on the ceiling. A mobile 8.5 cm ArUco marker is placed on the back of the leader, and the follower constructs the pseudo-pose measurements using the model described in Section IV-C2. The leader and follower

robots share the same IMU and WO noise specifications and initial covariance conditions. The stationary marker noise specifications are consistent with those in the previous section while the follower's marker measurement noise covariance is $R_{mf_1} = \text{diag}([0.0050\mathbf{I}_3 \text{ rad}^2, 0.0016\mathbf{I}_3 \text{ m}^2])$. The results of two tests are illustrated in Fig.10. The trajectories of robots under cornering motion as shown in Fig10-(a) and (c) demonstrate the overall improvement provided by the proposed method for both robots. The effectiveness of the method becomes particularly evident during abrupt decelerations and accelerations triggered by the control system (See Fig.10-(b)-(d)). In our experiments, sharp maneuvers were necessary to navigate corners due to the limited coverage area of the motion tracker and the cameras' restricted field of view. This led to the failure of the IMU/WO filter for the follower robot. However, the trajectory is successfully recovered by integrating FD with ArUco marker pseudo-measurements.

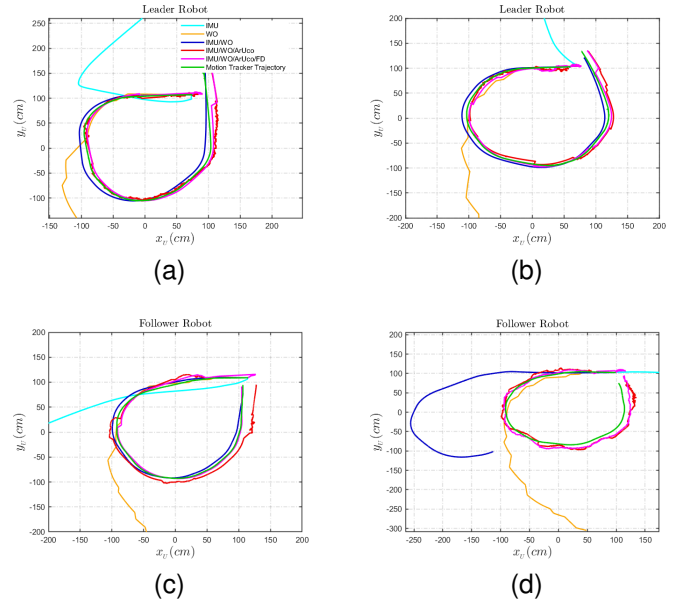


Fig. 10. Performance of the Leader-Follower localization framework.

3) *Multi-Robot Localization Results:* In these experiments, we use three robots to evaluate the scalability of the proposed method, as outlined in Section IV-C3. The leader observes a stationary 36 cm ArUco marker on the ceiling, while a follower type 1 (follower-1) tracks an 8.5 cm mobile ArUco marker on the leader. A follower type 2 (follower-2) tracks an 8.5 cm mobile ArUco marker on follower-1. The initial covariance and noise properties of the follower-2 are the same as follower-1. Two sets of experiments are presented in Fig.11. In both cases, we observe that uncertainty propagates and increases from the leader to follower-1 and follower-2 robots. In the first experiment (Fig.11-(a), (c), and (e)), when the IMU/WO filter provides good results for follower-1 and follower-2, but the ArUco marker measurements are less reliable, the FD modules filters out these measurements, and the final localization results closely match the ground truth trajectory for all robots. In the second set of experiments (Fig.11-(b), (d), and (f)), when the IMU/WO filter performs

poorly for follower-1 and fails for follower-2 due to sharp maneuvers, we observe that the proposed method can recover the ground truth trajectory with good precision.

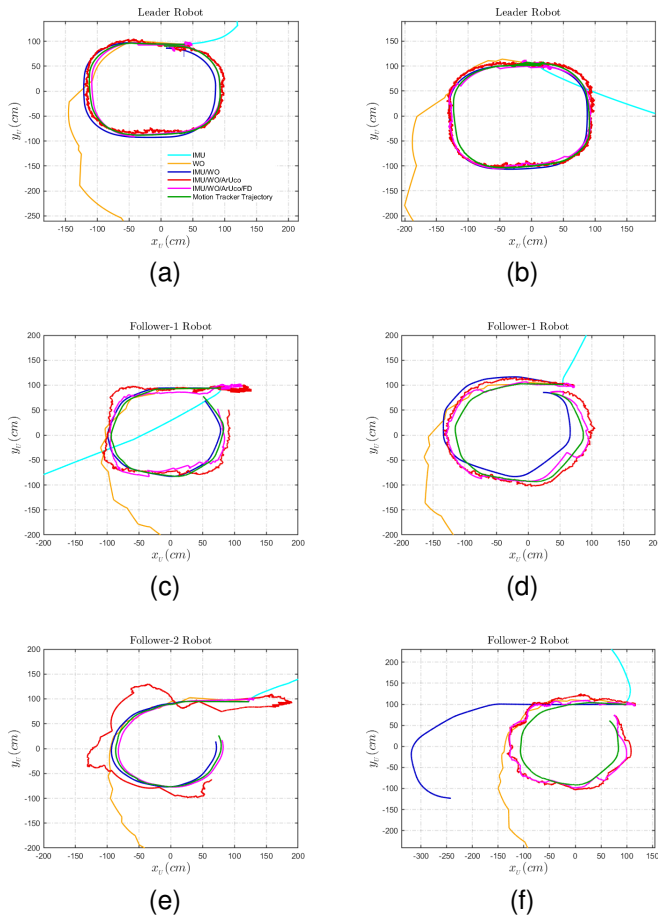


Fig. 11. Performance of the multi-robot localization framework.

4) *Fusion in Localization*: To demonstrate the effectiveness of fusion, we conducted tests in which follower-2 constructs two sets of pseudo-pose measurement based on the relative poses from two robots. Using these measurements, follower-2 generates two individual estimates of its own pose and combines them using the fusion operation described in Section III-E. The results for three experiments are shown in Fig. 12. Due to hardware limitations, these experiments were conducted only during near-straight motion. In all cases, the reference member required for fusion was calculated using averaging operation with $\alpha_1 = \alpha_2 = 0.5$. The results show that the overall performance of the fused estimate for follower-2 is better than the individual estimates and the IMU/WO filter.

VI. CONCLUSION

In this paper, we introduced stochastic operations on matrix Lie groups to perform operations such as composition, differencing, inverse, averaging, fusion, and constrained fusion on correlated estimates. We then applied them to develop a scalable multi-robot localization framework that integrated multi-modal sensor fusion (inertial, velocity, and pose measurements) and fault detection techniques. Experiments with

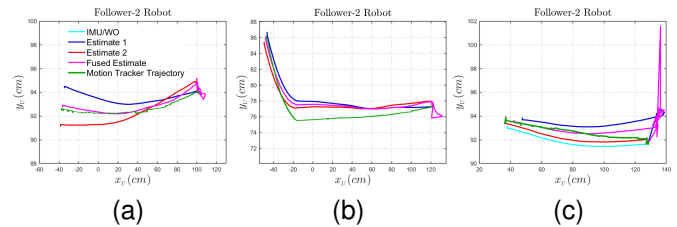


Fig. 12. Performance of fusion in the multi-robot localization framework.

a network of wheeled mobile robots equipped with IMUs, wheel encoders, and ArUco markers, demonstrated real-time, efficient, and reliable localization across the entire network. The experiments also revealed that the performance of the localization system was influenced by factors such as lighting conditions, robot speed and vibration, uneven terrain, marker size, abrupt maneuvers, and initial conditions. While the proposed system demonstrated significant advances, there are several directions for future work. Future work could focus on integrating diverse sensors such as LiDAR to improve accuracy. Enhancing the fault detection module with machine learning for better detection of faulty sensor readings and expanding the system to handle more sensor faults would further strengthen its long-term robustness. Additionally, scaling the method for larger robot networks in complex environments requires optimizing communication strategies to manage bandwidth limitations. Finally, adapting the framework for other robotic platforms, such as aerial or underwater robots, could address different localization challenges.

REFERENCES

- [1] Y.-S. Kwon and B.-J. Yi, "Design and motion planning of a two-module collaborative indoor pipeline inspection robot," *IEEE Transactions on Robotics*, vol. 28, no. 3, pp. 681–696, 2012.
- [2] M. Wang, B. Xin, M. Jing, and Y. Qu, "An exploration-enhanced search algorithm for robot indoor source searching," *IEEE Transactions on Robotics*, vol. 40, pp. 4160–4178, 2024.
- [3] B. Barshan and H. F. Durrant-Whyte, "Inertial navigation systems for mobile robots," *IEEE transactions on robotics and automation*, vol. 11, no. 3, pp. 328–342, 1995.
- [4] J. Borenstein and L. Feng, "Measurement and correction of systematic odometry errors in mobile robots," *IEEE Transactions on robotics and automation*, vol. 12, no. 6, pp. 869–880, 1996.
- [5] —, "Gyrodometry: A new method for combining data from gyros and odometry in mobile robots," in *Proceedings of IEEE International Conference on Robotics and Automation*, vol. 1. IEEE, 1996, pp. 423–428.
- [6] B.-S. Cho, W.-s. Moon, W.-J. Seo, and K.-R. Baek, "A dead reckoning localization system for mobile robots using inertial sensors and wheel revolution encoding," *Journal of mechanical science and technology*, vol. 25, pp. 2907–2917, 2011.
- [7] Q. Wang, M. Cai, and Z. Guo, "An enhanced positioning technique for underground pipeline robot based on inertial sensor/wheel odometer," *Measurement*, vol. 206, p. 112298, 2023.
- [8] M. Bloesch, S. Omari, P. Fankhauser, H. Sommer, C. Gehring, J. Hwangbo, M. A. Hoepflinger, M. Hutter, and R. Siegwart, "Fusion of optical flow and inertial measurements for robust egomotion estimation. in 2014 IEEE," in *IEEE/RSJ International Conference on Intelligent Robots and Systems*, 2014, pp. 3102–3107.
- [9] M. A. Shalaby, C. C. Cossette, J. Le Ny, and J. R. Forbes, "Multi-robot relative pose estimation and imu preintegration using passive uwb transceivers," *IEEE Transactions on Robotics*, vol. 40, pp. 2410–2429, 2024.

- [10] X. Liu, S. Wen, J. Zhao, T. Z. Qiu, and H. Zhang, "Edge-assisted multi-robot visual-inertial slam with efficient communication," *IEEE Transactions on Automation Science and Engineering*, vol. 22, pp. 2186–2198, 2024.
- [11] A. Perttula, H. Leppäkoski, M. Kirkko-Jaakkola, P. Davidson, J. Collin, and J. Takala, "Distributed indoor positioning system with inertial measurements and map matching," *IEEE Transactions on Instrumentation and Measurement*, vol. 63, no. 11, pp. 2682–2695, 2014.
- [12] R. Sharma and C. Taylor, "Cooperative navigation of mavs in gps denied areas," in *IEEE International Conference on Multisensor Fusion and Integration for Intelligent Systems*, 2008, pp. 481–486.
- [13] G. L. Mariottini, F. Morbidi, D. Prattichizzo, N. Vander Valk, N. Michael, G. Pappas, and K. Daniilidis, "Vision-based localization for leader–follower formation control," *IEEE Transactions on Robotics*, vol. 25, no. 6, pp. 1431–1438, 2009.
- [14] S. Van Der Helm, M. Coppola, K. N. McGuire, and G. C. De Croon, "On-board range-based relative localization for micro air vehicles in indoor leader–follower flight," *Autonomous Robots*, vol. 44, no. 3, pp. 415–441, 2020.
- [15] X. Fang, L. Xie, and X. Li, "Integrated relative-measurement-based network localization and formation maneuver control," *IEEE Transactions on Automatic Control*, vol. 69, no. 3, pp. 1906–1913, 2023.
- [16] A. Assa and F. Janabi-Sharifi, "A kalman filter-based framework for enhanced sensor fusion," *IEEE Sensors Journal*, vol. 15, no. 6, pp. 3281–3292, 2015.
- [17] L. Pedroso and P. Batista, "Distributed decentralized ekf for very large-scale networks with application to satellite mega-constellations navigation," *Control Engineering Practice*, vol. 135, p. 105509, 2023.
- [18] D. Kenwright and S. Blaylock, "Groups a path to geometry," University of Cambridge, Computer Laboratory, Tech. Rep., 2013, available at: <https://www.cl.cam.ac.uk/>.
- [19] R. P. Paul, *Robot manipulators: mathematics, programming, and control: the computer control of robot manipulators*. Richard Paul, 1981.
- [20] H. F. Durrant-Whyte, "Consistent integration and propagation of disparate sensor observations," *The International journal of robotics research*, vol. 6, no. 3, pp. 3–24, 1987.
- [21] S.-F. Su and C. G. Lee, "Manipulation and propagation of uncertainty and verification of applicability of actions in assembly tasks," *IEEE Transactions on Systems, Man, and Cybernetics*, vol. 22, no. 6, pp. 1376–1389, 1992.
- [22] Y. Wang and G. S. Chirikjian, "Error propagation on the euclidean group with applications to manipulator kinematics," *IEEE Transactions on Robotics*, vol. 22, no. 4, pp. 591–602, 2006.
- [23] G. S. Chirikjian, *Stochastic models, information theory, and Lie groups, volume 2: Analytic methods and modern applications*. Springer Science & Business Media, 2011, vol. 2.
- [24] C. Hertzberg, R. Wagner, U. Frese, and L. Schröder, "Integrating generic sensor fusion algorithms with sound state representations through encapsulation of manifolds," *Information Fusion*, vol. 14, no. 1, pp. 57–77, 2013.
- [25] A. W. Long, K. C. Wolfe, M. J. Mashner, G. S. Chirikjian *et al.*, "The banana distribution is gaussian: A localization study with exponential coordinates," *Robotics: Science and Systems VIII*, vol. 265, p. 1, 2013.
- [26] T. D. Barfoot and P. T. Furgale, "Associating uncertainty with three-dimensional poses for use in estimation problems," *IEEE Transactions on Robotics*, vol. 30, no. 3, pp. 679–693, 2014.
- [27] T. Y. Tang, D. J. Yoon, and T. D. Barfoot, "A white-noise-on-jerk motion prior for continuous-time trajectory estimation on se(3)," *IEEE Robotics and Automation Letters*, vol. 4, no. 2, pp. 594–601, 2019.
- [28] J. N. Wong, D. J. Yoon, A. P. Schoellig, and T. D. Barfoot, "A data-driven motion prior for continuous-time trajectory estimation on se(3)," *IEEE Robotics and Automation Letters*, vol. 5, no. 2, pp. 1429–1436, 2020.
- [29] J. G. Mangelson, M. Ghaffari, R. Vasudevan, and R. M. Eustice, "Characterizing the uncertainty of jointly distributed poses in the lie algebra," *IEEE Transactions on Robotics*, vol. 36, no. 5, pp. 1371–1388, 2020.
- [30] M. Brossard, A. Barrau, and S. Bonnabel, "Exploiting symmetries to design ekfs with consistency properties for navigation and slam," *IEEE Sensors Journal*, vol. 19, no. 4, pp. 1572–1579, 2018.
- [31] S. Heo and C. G. Park, "Consistent ekf-based visual-inertial odometry on matrix lie group," *IEEE Sensors Journal*, vol. 18, no. 9, pp. 3780–3788, 2018.
- [32] S. Bonnabel, "Left-invariant extended kalman filter and attitude estimation," in *IEEE Conference on Decision and Control*, 2007, pp. 1027–1032.
- [33] J. Xu, P. Zhu, and W. Ren, "Distributed invariant extended kalman filter for 3-d dynamic state estimation using lie groups," in *American Control Conference*, 2022, pp. 2367–2372.
- [34] A. M. Sjøberg and O. Egeland, "Lie algebraic unscented kalman filter for pose estimation," *IEEE Transactions on Automatic Control*, vol. 67, no. 8, pp. 4300–4307, 2021.
- [35] J. Bohn and A. K. Sanyal, "Unscented state estimation for rigid body motion on se(3)," in *IEEE Conference on Decision and Control*, 2012, pp. 7498–7503.
- [36] G. Marjanovic and V. Solo, "An engineer's guide to particle filtering on matrix lie groups," in *IEEE International Conference on Acoustics, Speech and Signal Processing*, 2016, pp. 3969–3973.
- [37] C. Forster, L. Carlone, F. Dellaert, and D. Scaramuzza, "On-manifold preintegration for real-time visual-inertial odometry," *IEEE Transactions on Robotics*, vol. 33, no. 1, pp. 1–21, 2016.
- [38] Drummond and Roussopoulos, "Computing map trajectories by representing, propagating and combining pdfs over groups," in *IEEE International Conference on Computer Vision*, 2003, pp. 1275–1282.
- [39] K. C. Wolfe, M. Mashner, and G. S. Chirikjian, "Bayesian fusion on lie groups," *Journal of Algebraic Statistics*, vol. 2, no. 1, 2011.
- [40] J. H. Hwang, J. Cha, and C. G. Park, "A novel federated structure of invariant ekf using left/right-invariant observations," *IEEE Sensors Journal*, vol. 22, no. 21, pp. 20645–20654, 2022.
- [41] M. E. Petersen, J. C. Ellingson, and R. W. Beard, "Tracking multiple unmanned aerial vehicles on se(3) using a monocular camera," *IEEE Transactions on Aerospace and Electronic Systems*, vol. 59, no. 4, pp. 3726–3735, 2022.
- [42] L. Li and M. Yang, "Joint localization based on split covariance intersection on the lie group," *IEEE Transactions on Robotics*, vol. 37, no. 5, pp. 1508–1524, 2021.
- [43] J. Xu, P. Zhu, Y. Zhou, and W. Ren, "Distributed invariant extended kalman filter using lie groups: Algorithm and experiments," *IEEE Transactions on Control Systems Technology*, vol. 31, no. 6, pp. 2777–2789, 2023.
- [44] M. Zarei and R. Chhabra, "Consistent fusion of correlated pose estimates on matrix lie groups," *IEEE Robotics and Automation Letters*, vol. 9, no. 7, pp. 6584–6591, 2024.
- [45] M. Brossard, S. Bonnabel, and A. Barrau, "Unscented kalman filter on lie groups for visual inertial odometry," in *IEEE/RSJ International Conference on Intelligent Robots and Systems*. IEEE, 2018, pp. 649–655.
- [46] S.-H. Tsao and S.-S. Jan, "Analytic imu preintegration that associates uncertainty on matrix lie groups for consistent visual-inertial navigation systems," *IEEE Robotics and Automation Letters*, vol. 8, no. 6, pp. 3820–3827, 2023.
- [47] S. Du, Y. Huang, B. Lin, J. Qian, and Y. Zhang, "A lie group manifold-based nonlinear estimation algorithm and its application to low-accuracy sins/gnss integrated navigation," *IEEE Transactions on Instrumentation and Measurement*, vol. 71, pp. 1–27, 2022.
- [48] P. Vial, J. Solà, N. Palomeras, and M. Carreras, "On lie group imu and linear velocity preintegration for autonomous navigation considering the earth rotation compensation," *IEEE Transactions on Robotics*, vol. 41, pp. 1346–1364, 2025.
- [49] X. Li and G. S. Chirikjian, "Lie-theoretic multi-robot localization," in *Riemannian Computing in Computer Vision*. Springer, 2016, pp. 165–186.
- [50] R. Dubois, A. Eudes, and V. Frémont, "Sharing visual-inertial data for collaborative decentralized simultaneous localization and mapping," *Robotics and Autonomous Systems*, vol. 148, p. 103933, 2022.
- [51] —, "On data sharing strategy for decentralized collaborative visual-inertial simultaneous localization and mapping," in *IEEE/RSJ International Conference on Intelligent Robots and Systems*, 2019, pp. 2123–2130.
- [52] J. Knuth and P. Barooah, "Distributed collaborative localization of multiple vehicles from relative pose measurements," in *47th Annual Allerton Conference on Communication, Control, and Computing*, 2009, pp. 314–321.
- [53] G. Shin, H. Sim, S. Nam, Y. Kim, J. Heo, and K.-K. K. Kim, "Multi-robot relative pose estimation in se(2) with observability analysis: A comparison of extended kalman filtering and robust pose graph optimization," *IEEE Transactions on Intelligent Vehicles*, pp. 1–23, 2024.
- [54] Y. Zhou, Y. Liu, P. Zhu, and X. Wang, "Distributed invariant kalman filter for cooperative localization using matrix lie groups," *arXiv preprint arXiv:2405.04000*, 2024.
- [55] H. Li, Q. Zeng, H. Li, Y. Zhang, and J. Wu, "Distributed invariant kalman filter for object-level multi-robot pose slam," *arXiv preprint arXiv:2409.09410*, 2024.

- [56] M. Kalaitzakis, B. Cain, S. Carroll, A. Ambrosi, C. Whitehead, and N. Vitzilaios, "Fiducial markers for pose estimation: Overview, applications and experimental comparison of the artag, apriltag, aruco and stag markers," *Journal of Intelligent & Robotic Systems*, vol. 101, pp. 1–26, 2021.
- [57] M. Fourmy, D. Atchuthan, N. Mansard, J. Sola, and T. Flayols, "Absolute humanoid localization and mapping based on imu lie group and fiducial markers," in *IEEE/RAS 19th International Conference on Humanoid Robots*, 2019, pp. 237–243.
- [58] J. Zheng, S. Bi, B. Cao, and D. Yang, "Visual localization of inspection robot using extended kalman filter and aruco markers," in *IEEE International Conference on Robotics and Biomimetics*, 2018, pp. 742–747.
- [59] X. Li, S. Patel, D. Stronzek-Pfeifer, and C. Büskens, "Indoor localization for an autonomous model car: A marker-based multi-sensor fusion framework," in *IEEE 19th International Conference on Automation Science and Engineering*, 2023, pp. 1–8.
- [60] A. Joon and W. Kowalczyk, "Leader-follower approach for non-holonomic mobile robots based on extended kalman filter sensor data fusion and extended on-board camera perception controlled with behavior tree," *Sensors*, vol. 23, no. 21, p. 8886, 2023.
- [61] Z. Zhou, W. Tang, Z. Wang, L. Wang, and R. Zhang, "Multi-robot real-time cooperative localization based on high-speed feature detection and two-stage filtering," in *IEEE International Conference on Real-time Computing and Robotics*, 2021, pp. 690–696.
- [62] Z. Li, R. Acuna, and V. Willert, "Cooperative localization by fusing pose estimates from static environmental and mobile fiducial features," in *Latin American Robotic Symposium, Brazilian Symposium on Robotics and Workshop on Robotics in Education*. IEEE, 2018, pp. 65–70.
- [63] M. Shan, Y. Zou, M. Guan, C. Wen, K.-Y. Lim, C.-L. Ng, and P. Tan, "Probabilistic trajectory estimation based leader following for multi-robot systems," in *14th International Conference on Control, Automation, Robotics and Vision*. IEEE, 2016, pp. 1–6.
- [64] S. Oh-hara and A. Fujimori, "A leader-follower formation control of mobile robots by position-based visual servo method using fisheye camera," *ROBOMECH Journal*, vol. 10, no. 1, p. 30, 2023.
- [65] D. Jayarathne, H. Vidumal, S. Senevirathne, P. Jayasekara, and T. Lalitharatne, "Vision-based leader-follower mobile robots for cooperative object handling," in *19th International Conference on Control, Automation and Systems*. IEEE, 2019, pp. 747–752.
- [66] A. Barrau, "Non-linear state error based extended kalman filters with applications to navigation," Ph.D. dissertation, Mines Paristech, 2015.
- [67] R. M. Murray, Z. Li, and S. S. Sastry, *A mathematical introduction to robotic manipulation*. CRC press, 2017.
- [68] T. D. Barfoot, *State estimation for robotics*. Cambridge University Press, 2017.
- [69] G. Bourmaud, R. Mégret, M. Arnaudon, and A. Giremus, "Continuous-discrete extended kalman filter on matrix lie groups using concentrated gaussian distributions," *Journal of Mathematical Imaging and Vision*, vol. 51, pp. 209–228, 2015.
- [70] G. Bourmaud, R. Mégret, A. Giremus, and Y. Berthoumieu, "Discrete extended kalman filter on lie groups," in *European Signal Processing Conference*, 2013, pp. 1–5.
- [71] T. K. Moon and W. C. Stirling, *Mathematical methods and algorithms for signal processing*. Prentice hall Upper Saddle River, NJ, 2000, vol. 1.
- [72] P. C. Mahalanobis, "On tests and measures of group divergence," *J. Asiat. Soc. Bengal*, vol. 26, pp. 541–588, 1930.
- [73] R. Lin, E. Khalastchi, and G. A. Kaminka, "Detecting anomalies in unmanned vehicles using the mahalanobis distance," in *IEEE international conference on robotics and automation*, 2010, pp. 3038–3044.
- [74] "Phasespace motion capture," accessed: 2025-02-05. [Online]. Available: <https://www.phasespace.com/>
- [75] "Agilex limo robot," accessed: 2025-02-05. [Online]. Available: <https://global.agilex.ai/products/limo-pro>
- [76] "Camera calibration," accessed: 2025-02-05. [Online]. Available: http://wiki.ros.org/camera_calibration
- [77] "The aruco ros library," accessed: 2025-02-05. [Online]. Available: http://wiki.ros.org/aruco_ros

APPENDIX A

PROPERTIES OF THE DEVELOPED LIE GROUP $\mathcal{G}_{\mathcal{X}}$

We begin by showing $\mathcal{G}_{\mathcal{X}}$ is a matrix Lie group, i.e., verifying its closure, associativity, and the existence of identity

and inverse elements. To this end, we first observe that the Lie group $\mathcal{G}_{\mathcal{X}} := \mathbb{SE}_2(3) \times \mathbb{R}^3 \times \mathbb{R}^3$ is a special case of Lie group:

$$\mathcal{G} := \left\{ \mathcal{X} = \begin{bmatrix} \mathfrak{X}_1 & \mathbf{0}_5 \\ \mathbf{0}_5 & \mathfrak{X}_2 \end{bmatrix} \mid \mathfrak{X}_1, \mathfrak{X}_2 \in \mathbb{SE}_2(3) \right\}, \quad (60)$$

when the rotation angle in \mathfrak{X}_2 is zero. We therefore establish the proofs for the \mathcal{G} . For closure, we show the set of matrices in the Lie group \mathcal{G} is closed under matrix multiplication, i.e., if $\mathcal{X} = \begin{bmatrix} \mathfrak{X}_1 & \mathbf{0}_5 \\ \mathbf{0}_5 & \mathfrak{X}_2 \end{bmatrix} \in \mathcal{G}$, $\mathcal{Y} = \begin{bmatrix} \mathfrak{Y}_1 & \mathbf{0}_5 \\ \mathbf{0}_5 & \mathfrak{Y}_2 \end{bmatrix} \in \mathcal{G}$, then $\mathcal{Z} = \mathcal{X}\mathcal{Y} \in \mathcal{G}$.

Specifically, we have $\mathcal{Z} = \mathcal{X}\mathcal{Y} = \begin{bmatrix} \mathfrak{X}_1\mathfrak{Y}_1 & \mathbf{0}_5 \\ \mathbf{0}_5 & \mathfrak{X}_2\mathfrak{Y}_2 \end{bmatrix}$. Since $\mathfrak{X}_1\mathfrak{Y}_1 \in \mathbb{SE}_2(3)$ and $\mathfrak{X}_2\mathfrak{Y}_2 \in \mathbb{SE}_2(3)$, therefore $\mathcal{Z} \in \mathcal{G}$. The inverse elements of \mathcal{G} is calculated as $\mathcal{X}^{-1} = \begin{bmatrix} \mathfrak{X}_1^{-1} & \mathbf{0}_5 \\ \mathbf{0}_5 & \mathfrak{X}_2^{-1} \end{bmatrix}$. Since $\mathfrak{X}_1^{-1}, \mathfrak{X}_2^{-1} \in \mathbb{SE}_2(3)$, we conclude $\mathcal{X}^{-1} \in \mathcal{G}$. The identity element of \mathcal{G} is \mathbf{I}_{10} and the associativity of the matrix Lie group \mathcal{G} follows trivially from the associativity of matrix multiplication. For a block real squared matrix $\mathbf{M} = \begin{bmatrix} \mathbf{M}_1 & \mathbf{0}_n \\ \mathbf{0}_n & \mathbf{M}_2 \end{bmatrix}$ we have $\exp(\mathbf{M}) = \begin{bmatrix} \exp(\mathbf{M}_1) & \mathbf{0}_n \\ \mathbf{0}_n & \exp(\mathbf{M}_2) \end{bmatrix}$, which verifies that $\mathcal{X} = \begin{bmatrix} \mathfrak{X}_1 & \mathbf{0}_5 \\ \mathbf{0}_5 & \mathfrak{X}_2 \end{bmatrix} = \begin{bmatrix} \exp([\xi_1]_{\wedge}) & \mathbf{0}_5 \\ \mathbf{0}_5 & \exp([\xi_2]_{\wedge}) \end{bmatrix} = \exp([\zeta]_{\wedge})$ with $[\zeta]_{\wedge}$ being an element of Lie algebra of \mathcal{G} given by

$$\mathfrak{g} := \left\{ [\zeta]_{\wedge} = \begin{bmatrix} [\xi_1]_{\wedge} & \mathbf{0}_5 \\ \mathbf{0}_5 & [\xi_2]_{\wedge} \end{bmatrix} \mid [\xi_1]_{\wedge}, [\xi_2]_{\wedge} \in \mathfrak{so}_2(3) \right\}, \quad (61)$$

where, $\zeta = [\xi_1^{\top} \ \xi_2^{\top}]^{\top} \in \mathbb{R}^{18}$. The Lie algebra of $\mathcal{G}_{\mathcal{X}}$, denoted as $\mathfrak{g}_{\mathcal{X}}$, is a special case of \mathfrak{g} when rotation angle in ξ_2 is zero. From the definitions $\text{Ad}_{\mathcal{X}}(\zeta) := [\mathcal{X} [\zeta]_{\wedge} \mathcal{X}^{-1}]_{\vee}$ and $\text{ad}_{\zeta}(\eta) := [[\zeta]_{\wedge}, [\eta]_{\wedge}]_{\vee}$ we obtain

$$\text{Ad}_{\mathcal{X}} = \begin{bmatrix} \text{Ad}_{\mathfrak{X}_1} & \mathbf{0}_9 \\ \mathbf{0}_9 & \text{Ad}_{\mathfrak{X}_2} \end{bmatrix} \in \mathbb{R}^{18 \times 18}, \quad (62)$$

$$\text{ad}_{\zeta} = \begin{bmatrix} \text{ad}_{\xi_1} & \mathbf{0}_9 \\ \mathbf{0}_9 & \text{ad}_{\xi_2} \end{bmatrix} \in \mathbb{R}^{18 \times 18}. \quad (63)$$

Moreover, the inverse of the right Jacobian of the group \mathcal{G} is

$$\begin{aligned} \mathcal{J}_r^{-1}(\zeta) &= \sum_{n=0}^{\infty} \frac{B_n}{n!} (-\text{ad}_{\zeta})^n \\ &= \begin{bmatrix} \sum_{n=0}^{\infty} \frac{B_n}{n!} (-\text{ad}_{\xi_1})^n & \mathbf{0}_{18} \\ \mathbf{0}_{18} & \sum_{n=0}^{\infty} \frac{B_n}{n!} (-\text{ad}_{\xi_2})^n \end{bmatrix} \\ &= \begin{bmatrix} \mathcal{J}_r^{-1}(\xi_1) & \mathbf{0}_{18} \\ \mathbf{0}_{18} & \mathcal{J}_r^{-1}(\xi_2) \end{bmatrix}, \end{aligned} \quad (64)$$

where, $\mathcal{J}_r^{-1}(\xi_i)$ is the inverse of the right Jacobian of the $\mathbb{SE}_2(3)$ for $i \in \{1, 2\}$. The proofs for the Lie group $\mathcal{G}_{\mathcal{Z}} := \mathbb{SE}(3) \times \mathbb{R}^3$ follows a similar procedure and is left to the reader.

APPENDIX B

PROOF OF INVERSE OPERATION

We let the inverse of the stochastic member $\mathcal{X} = \bar{\mathcal{X}} \exp([\zeta]_{\wedge})$ with $\zeta \sim \mathcal{N}(\mathbf{0}, \mathbf{P})$ to be $\mathcal{X}_{\text{inv}} = \mathcal{X}^{-1}$. Thus,

$$\mathcal{X}_{\text{inv}}^{-1} = \bar{\mathcal{X}} \exp([\zeta]_{\wedge}) = \exp([\text{Ad}_{\bar{\mathcal{X}}}\zeta]_{\wedge}) \bar{\mathcal{X}}. \quad (65)$$

Taking the inverse $\mathcal{X}_{\text{inv}} = \bar{\mathcal{X}}^{-1} \exp(-[\text{Ad}_{\bar{\mathcal{X}}}\zeta]_{\wedge})$. Thus, mean and covariance of $\mathcal{X}_{\text{inv}} = \bar{\mathcal{X}}_{\text{inv}} \exp([\zeta]_{\text{inv}})_{\wedge}$ are

$$\bar{\mathcal{X}}_{\text{inv}} = \bar{\mathcal{X}}^{-1}, \quad (66)$$

$$\zeta_{\text{inv}} = -\text{Ad}_{\bar{\mathcal{X}}}\zeta, \quad (67)$$

$$\mathbf{P}_{\text{inv}} = \mathbb{E}[\zeta_{\text{inv}}\zeta_{\text{inv}}^{\top}] = \text{Ad}_{\bar{\mathcal{X}}}\mathbb{E}[\zeta\zeta^{\top}]\text{Ad}_{\bar{\mathcal{X}}}^{\top} = \text{Ad}_{\bar{\mathcal{X}}}\mathbf{P}\text{Ad}_{\bar{\mathcal{X}}}^{\top}. \quad (68)$$

APPENDIX C

PROOF OF COMPOSITION OPERATION

The proof is realized by induction. For the base step, i.e., $n = 2$, the two stochastic members are defined as $\mathcal{X}_1 = \bar{\mathcal{X}}_1 \exp([\zeta_1]_{\wedge})$ and $\mathcal{X}_2 = \bar{\mathcal{X}}_2 \exp([\zeta_2]_{\wedge})$ with $\zeta_1 \sim \mathcal{N}(\mathbf{0}, \mathbf{P}_{11})$ and $\zeta_2 \sim \mathcal{N}(\mathbf{0}, \mathbf{P}_{22})$, respectively. Then we have

$$\mathcal{X}_{\text{com}}^{(1)} = \mathcal{X}_1 \mathcal{X}_2 = \bar{\mathcal{X}}_1 \exp([\zeta_1]_{\wedge}) \bar{\mathcal{X}}_2 \exp([\zeta_2]_{\wedge}). \quad (69)$$

Next, we compute the inverse of $\mathcal{X}_{\text{com}}^{(1)}$ as

$$(\mathcal{X}_{\text{com}}^{(1)})^{-1} = \exp([-\zeta_2]_{\wedge}) \bar{\mathcal{X}}_2^{-1} \exp([-\zeta_1]_{\wedge}) \bar{\mathcal{X}}_1^{-1}.$$

Based on the definition of the Adjoint mapping we obtain

$$(\mathcal{X}_{\text{com}}^{(1)})^{-1} = \exp([-\zeta_2]_{\wedge}) \exp([- \text{Ad}_{\bar{\mathcal{X}}_2^{-1}} \zeta_1]_{\wedge}) \bar{\mathcal{X}}_2^{-1} \bar{\mathcal{X}}_1^{-1},$$

which results in

$$\mathcal{X}_{\text{com}}^{(1)} = \bar{\mathcal{X}}_1 \bar{\mathcal{X}}_2 \exp([\text{Ad}_{\bar{\mathcal{X}}_2^{-1}} \zeta_1]_{\wedge}) \exp([\zeta_2]_{\wedge}). \quad (70)$$

Thus, the mean and uncertainty vector of $\mathcal{X}_{\text{com}}^{(1)} = \bar{\mathcal{X}}_{\text{com}}^{(1)} \exp([\zeta_{\text{com}}^{(1)}]_{\wedge})$ considering the BCH first-order terms are

$$\bar{\mathcal{X}}_{\text{com}}^{(1)} = \bar{\mathcal{X}}_1 \bar{\mathcal{X}}_2, \quad (71)$$

$$\zeta_{\text{com}}^{(1)} \approx \zeta_2 + \text{Ad}_{\bar{\mathcal{X}}_2^{-1}} \zeta_1. \quad (72)$$

Assuming the independence of ζ_1 and ζ_2 , the covariance of $\mathcal{X}_{\text{com}}^{(1)}$ is calculated as

$$\mathbf{P}_{\text{com}}^{(1)} = \mathbb{E}[\zeta_{\text{com}}^{(1)} (\zeta_{\text{com}}^{(1)})^{\top}] \approx \mathbf{P}_{22} + \text{Ad}_{\bar{\mathcal{X}}_2^{-1}} \mathbf{P}_{11} \text{Ad}_{\bar{\mathcal{X}}_2^{-1}}^{\top}. \quad (73)$$

In the inductive step, we assume the following statement holds for some arbitrary $n = k$, i.e.,

$$\begin{aligned} \mathcal{X}_{\text{com}}^{(k)} &= \bar{\mathcal{X}}_1 \bar{\mathcal{X}}_2 \cdots \bar{\mathcal{X}}_{k-1} \bar{\mathcal{X}}_k \exp([\text{Ad}_{\bar{\mathcal{X}}_{k-1} \cdots \bar{\mathcal{X}}_2^{-1}} \zeta_1]_{\wedge}) \\ &\quad \exp([\text{Ad}_{\bar{\mathcal{X}}_{k-1} \cdots \bar{\mathcal{X}}_3^{-1}} \zeta_2]_{\wedge}) \cdots \exp([\text{Ad}_{\bar{\mathcal{X}}_k^{-1}} \zeta_{k-1}]_{\wedge}) \\ &\quad \exp([\zeta_k]_{\wedge}). \end{aligned}$$

Using the first-order terms of the BCH formula and assuming uncorrelated members, we obtain

$$\bar{\mathcal{X}}_{\text{com}}^{(k)} = \bar{\mathcal{X}}_1 \bar{\mathcal{X}}_2 \cdots \bar{\mathcal{X}}_{k-1} \bar{\mathcal{X}}_k, \quad (74)$$

$$\begin{aligned} \zeta_{\text{com}}^{(k)} &\approx \zeta_k + \text{Ad}_{\bar{\mathcal{X}}_k^{-1}} \zeta_{k-1} + \cdots \\ &\quad + \text{Ad}_{\bar{\mathcal{X}}_k^{-1} \cdots \bar{\mathcal{X}}_3^{-1}} \zeta_2 + \text{Ad}_{\bar{\mathcal{X}}_k^{-1} \cdots \bar{\mathcal{X}}_2^{-1}} \zeta_1, \end{aligned} \quad (75)$$

$$\begin{aligned} \mathbf{P}_{\text{com}}^{(k)} &\approx \mathbf{P}_{kk} + \text{Ad}_{\bar{\mathcal{X}}_k^{-1}} \mathbf{P}_{k-1k-1} \text{Ad}_{\bar{\mathcal{X}}_k^{-1}}^{\top} + \cdots \\ &\quad + \text{Ad}_{\bar{\mathcal{X}}_k^{-1} \cdots \bar{\mathcal{X}}_3^{-1}} \mathbf{P}_{22} \text{Ad}_{\bar{\mathcal{X}}_k^{-1} \cdots \bar{\mathcal{X}}_3^{-1}}^{\top} \\ &\quad + \text{Ad}_{\bar{\mathcal{X}}_k^{-1} \cdots \bar{\mathcal{X}}_2^{-1}} \mathbf{P}_{11} \text{Ad}_{\bar{\mathcal{X}}_k^{-1} \cdots \bar{\mathcal{X}}_2^{-1}}^{\top}. \end{aligned} \quad (76)$$

Next, the validity is shown for $n = k + 1$. We have

$$\mathcal{X}_{\text{com}}^{(k+1)} = \mathcal{X}_1 \cdots \mathcal{X}_k \mathcal{X}_{k+1} = \mathcal{X}_{\text{com}}^{(k)} \mathcal{X}_{k+1}. \quad (77)$$

This can be expanded as

$$\mathcal{X}_{\text{com}}^{(k+1)} = \bar{\mathcal{X}}_{\text{com}}^{(k)} \exp([\zeta_{\text{com}}^{(k)}]_{\wedge}) \bar{\mathcal{X}}_{k+1} \exp([\zeta_{k+1}]_{\wedge}), \quad (78)$$

and based on the result developed in (70) we obtain

$$\mathcal{X}_{\text{com}}^{(k+1)} = \bar{\mathcal{X}}_{\text{com}}^{(k)} \bar{\mathcal{X}}_{k+1} \exp([\text{Ad}_{\bar{\mathcal{X}}_{k+1}^{-1}} \zeta_{\text{com}}^{(k)}]_{\wedge}) \exp([\zeta_{k+1}]_{\wedge}).$$

Therefore, the mean and uncertainty vector of $\mathcal{X}_{\text{com}}^{(k+1)}$ are

$$\bar{\mathcal{X}}_{\text{com}}^{(k+1)} = \bar{\mathcal{X}}_{\text{com}}^{(k)} \bar{\mathcal{X}}_{k+1} = \bar{\mathcal{X}}_1 \cdots \bar{\mathcal{X}}_k \bar{\mathcal{X}}_{k+1} \quad (79)$$

$$\begin{aligned} \zeta_{\text{com}}^{(k+1)} &\approx \zeta_{k+1} + \text{Ad}_{\bar{\mathcal{X}}_{k+1}^{-1}} \zeta_{\text{com}}^{(k)} \\ &= \zeta_{k+1} + \text{Ad}_{\bar{\mathcal{X}}_{k+1}^{-1}} \zeta_k + \text{Ad}_{\bar{\mathcal{X}}_{k+1}^{-1}} \text{Ad}_{\bar{\mathcal{X}}_k^{-1}} \zeta_{k-1} \\ &\quad + \cdots + \text{Ad}_{\bar{\mathcal{X}}_{k+1}^{-1}} \text{Ad}_{\bar{\mathcal{X}}_k^{-1} \cdots \bar{\mathcal{X}}_2^{-1}} \zeta_1. \end{aligned} \quad (80)$$

Knowing $\text{Ad}_{\mathcal{X}\mathcal{Y}} = \text{Ad}_{\mathcal{X}} \text{Ad}_{\mathcal{Y}}$, and considering the first-order terms in the BCH we obtain

$$\begin{aligned} \zeta_{\text{com}}^{(k+1)} &\approx \zeta_{k+1} + \text{Ad}_{\bar{\mathcal{X}}_{k+1}^{-1}} \zeta_k + \text{Ad}_{\bar{\mathcal{X}}_{k+1}^{-1}} \bar{\mathcal{X}}_k^{-1} \zeta_{k-1} \\ &\quad + \cdots + \text{Ad}_{\bar{\mathcal{X}}_{k+1}^{-1}} \bar{\mathcal{X}}_k^{-1} \cdots \bar{\mathcal{X}}_2^{-1} \zeta_1. \end{aligned} \quad (81)$$

Assuming the independence of ζ_{k+1} , and $\zeta_{\text{com}}^{(k)}$, the covariance of $\mathcal{X}_{\text{com}}^{(k+1)}$ is calculated as

$$\begin{aligned} \mathbf{P}_{\text{com}}^{(k+1)} &\approx \mathbf{P}_{k+1k+1} + \text{Ad}_{\bar{\mathcal{X}}_{k+1}^{-1}} \mathbf{P}_{kk} \text{Ad}_{\bar{\mathcal{X}}_{k+1}^{-1}}^{\top} \\ &\quad \text{Ad}_{\bar{\mathcal{X}}_{k+1}^{-1}} \bar{\mathcal{X}}_k^{-1} \mathbf{P}_{k-1k-1} \text{Ad}_{\bar{\mathcal{X}}_{k+1}^{-1}}^{\top} \bar{\mathcal{X}}_k^{-1} + \cdots \\ &\quad + \text{Ad}_{\bar{\mathcal{X}}_{k+1}^{-1}} \bar{\mathcal{X}}_k^{-1} \cdots \bar{\mathcal{X}}_2^{-1} \mathbf{P}_{11} \text{Ad}_{\bar{\mathcal{X}}_{k+1}^{-1}}^{\top} \bar{\mathcal{X}}_k^{-1} \cdots \bar{\mathcal{X}}_2^{-1}. \end{aligned} \quad (82)$$

This completes the proof for uncorrelated configurations. When the stochastic configurations are correlated, it implies that the uncertainties associated with them are correlated, i.e., $\mathbb{E}[\zeta_i \zeta_j^{\top}] \neq \mathbf{0}_m$ for $i, j \in \{1, \dots, n\}$. In this case, we write the uncertainty vector as

$$\zeta_{\text{com}} = \begin{bmatrix} \mathbf{I}_m & \mathbf{0}_m & \cdots & \mathbf{0}_m \\ \mathbf{0}_m & \text{Ad}_{\bar{\mathcal{X}}_n^{-1}} & \cdots & \mathbf{0}_m \\ \vdots & \vdots & \ddots & \vdots \\ \mathbf{0}_m & \mathbf{0}_m & \cdots & \text{Ad}_{\bar{\mathcal{X}}_n^{-1} \cdots \bar{\mathcal{X}}_2^{-1}} \end{bmatrix} \begin{bmatrix} \zeta_n \\ \zeta_{n-1} \\ \vdots \\ \zeta_1 \end{bmatrix} = \mathcal{M} \zeta.$$

The covariance is then calculated as

$$\mathbf{P}_{\text{com}} = \mathbb{E}[\zeta_{\text{com}} \zeta_{\text{com}}^{\top}] \approx \mathcal{M} \mathbb{E}[\zeta \zeta^{\top}] \mathcal{M}^{\top}.$$

We let $\mathbf{P}_{ij} = \mathbb{E}[\zeta_i \zeta_j^{\top}]$ for $i, j \in \{1, \dots, n\}$, then

$$\mathbf{P}_{\text{com}} \approx \mathcal{M} \begin{bmatrix} \mathbf{P}_{nn} & \mathbf{P}_{nn-1} & \cdots & \mathbf{P}_{n1} \\ \mathbf{P}_{n-1n} & \mathbf{P}_{n-1n-1} & \cdots & \mathbf{P}_{n-11} \\ \vdots & \vdots & \ddots & \vdots \\ \mathbf{P}_{1n} & \mathbf{P}_{1n-1} & \cdots & \mathbf{P}_{11} \end{bmatrix} \mathcal{M}^{\top}.$$

APPENDIX D

PROOF OF DIFFERENCE OPERATION

Based on the difference definition we have $\mathcal{X}_{\text{dif}} = \mathcal{X}_1^{-1} \mathcal{X}_2$. We let $\mathcal{Y} = \mathcal{X}_1^{-1}$ and use the inverse operation to get

$$\mathcal{Y} = \bar{\mathcal{Y}} \exp([\zeta_{\mathcal{Y}}]_{\wedge}) = \bar{\mathcal{X}}_1^{-1} \exp(-[\text{Ad}_{\bar{\mathcal{X}}_1} \zeta_1]_{\wedge}). \quad (83)$$

We therefore have $\mathcal{X}_{\text{dif}} = \bar{\mathcal{Y}} \exp([\zeta_{\mathcal{Y}}]_{\wedge}) \bar{\mathcal{X}}_2 \exp([\zeta_2]_{\wedge})$. Using the composition rule results in

$$\bar{\mathcal{X}}_{\text{dif}} = \bar{\mathcal{Y}} \bar{\mathcal{X}}_2 = \bar{\mathcal{X}}_1^{-1} \bar{\mathcal{X}}_2, \quad (84)$$

$$\begin{aligned} \zeta_{\text{dif}} &\approx \zeta_2 + \text{Ad}_{\bar{\mathcal{X}}_2^{-1}} \zeta_{\mathcal{Y}} = \zeta_2 - \text{Ad}_{\bar{\mathcal{X}}_2^{-1}} \text{Ad}_{\bar{\mathcal{X}}_1} \zeta_1 \\ &= \zeta_2 - \text{Ad}_{\bar{\mathcal{X}}_2^{-1} \bar{\mathcal{X}}_1} \zeta_1, \end{aligned} \quad (85)$$

$$\begin{aligned} \mathbf{P}_{\text{dif}} &= \mathbb{E}[\zeta_{\text{dif}} \zeta_{\text{dif}}^{\top}] \approx \mathbf{P}_{22} - \mathbf{P}_{12} \text{Ad}_{\bar{\mathcal{X}}_2^{-1}} \bar{\mathcal{X}}_1^{-1} - \text{Ad}_{\bar{\mathcal{X}}_2^{-1} \bar{\mathcal{X}}_1} \mathbf{P}_{12} \\ &\quad + \text{Ad}_{\bar{\mathcal{X}}_2^{-1} \bar{\mathcal{X}}_1} \mathbf{P}_{11} \text{Ad}_{\bar{\mathcal{X}}_2^{-1} \bar{\mathcal{X}}_1}^{\top}. \end{aligned} \quad (86)$$

APPENDIX E
CONSTRAINED FUSION DERIVATION

For $\tilde{\mathbf{g}}(\zeta_c) = \mathbf{\Gamma}\zeta_c$ the Lagrangian reduces to:

$$\mathcal{L} = (\zeta_u + \mathcal{J}_r^{-1}(\zeta_u)\zeta_c)^\top \mathbf{W}_c (\zeta_u + \mathcal{J}_r^{-1}(\zeta_u)\zeta_c) + 2\boldsymbol{\lambda}^\top (\mathbf{\Gamma}\zeta_c - \tilde{\mathbf{d}}),$$

and therefore its derivatives with respect to ζ_c and $\boldsymbol{\lambda}$ are

$$\mathcal{J}_r^{-\top}(\zeta_u)\mathbf{W}_c(\zeta_u + \mathcal{J}_r^{-1}(\zeta_u)\zeta_c) + \mathbf{\Gamma}^\top \boldsymbol{\lambda} = \mathbf{0}_{m \times 1}, \quad (87)$$

$$\mathbf{\Gamma}\zeta_c - \tilde{\mathbf{d}} = \mathbf{0}_{r \times 1}. \quad (88)$$

From (87) we obtain

$$\zeta_c = -\mathfrak{J}(\mathcal{J}_r^{-\top}(\zeta_u)\mathbf{W}_c\zeta_u + \mathbf{\Gamma}^\top \boldsymbol{\lambda}), \quad (89)$$

where $\mathfrak{J} = (\mathcal{J}_r^{-\top}(\zeta_u)\mathbf{W}_c\mathcal{J}_r^{-1}(\zeta_u))^{-1}$. Substituting (89) in (88) and solving for $\boldsymbol{\lambda}$ gives $\boldsymbol{\lambda} = -(\mathbf{\Gamma}\mathfrak{J}\mathbf{\Gamma}^\top)^{-1}(\mathbf{\Gamma}\mathfrak{J}\mathcal{J}_r^{-\top}(\zeta_u)\mathbf{W}_c\zeta_u + \tilde{\mathbf{d}})$. Finally, by substituting the calculated $\boldsymbol{\lambda}$ in (89) and rearranging the terms, it is verified

$$\zeta_c = \mathfrak{J} \left[\left(\mathbf{\Gamma}^\top (\mathbf{\Gamma}\mathfrak{J}\mathbf{\Gamma}^\top)^{-1} \mathbf{\Gamma}\mathfrak{J}\mathcal{J}_r^{-\top}(\zeta_u)\mathbf{W}_c - \mathcal{J}_r^{-\top}(\zeta_u)\mathbf{W}_c \right) \zeta_u + \mathbf{\Gamma}^\top (\mathbf{\Gamma}\mathfrak{J}\mathbf{\Gamma}^\top)^{-1} \tilde{\mathbf{d}} \right]. \quad (90)$$